# Open Research Online
The Open University's repository of research publications
and other research outputs

# Drivers of late Miocene tropical sea surface cooling: a new perspective from the equatorial Indian Ocean

## Journal Item

For guidance on citations see FAQs.

Version: Accepted Manuscript

## oro.open.ac.uk

# Drivers of late Miocene tropical sea surface cooling: a new perspective from the equatorial Indian Ocean

**Claire Martinot[1], Clara T. Bolton[1], Anta-Clarisse Sarr[1], Yannick Donnadieu[1], Marta Garcia[1], Emmeline Gray[1,2], Kazuyo Tachikawa[1]**

[1]Aix Marseille Univ, CNRS, IRD, INRAE, Coll France, CEREGE, Aix-en-Provence, France

[2]Now at: School of Environment, Earth and Ecosystem Sciences, The Open University, Milton Keynes, UK

Corresponding authors: Claire Martinot (clairemartinot1@gmail.com) or Clara Bolton (bolton@cerege.fr)

**Key Points:**

- New late Miocene orbital-resolution Mg/Ca sea surface temperature record from the eastern equatorial Indian Ocean spanning 9 to 5 Ma

- Tropical cooling is >3°C; new model simulations suggest that a pCO2 decrease from 560 to 300 ppm could account for most of this cooling

- Increase in meridional sea surface temperature gradients over the late Miocene more modest than previously suggested

## Abstract

During the late Miocene, global cooling occurred alongside the establishment of near-modern terrestrial and marine ecosystems. Significant (3 to 5 °C) sea surface cooling from 7.5 to 5.5 Ma is recorded by proxies at mid to high latitudes, yet the magnitude of tropical cooling and the role of atmospheric carbon dioxide ($pCO_2$) in driving this trend are debated. Here, we present a new orbital-resolution sea surface temperature (SST) record spanning the late Miocene to earliest Pliocene (9 to 5 Ma) from the eastern equatorial Indian Ocean (International Ocean Discovery Program Site U1443) based on Mg/Ca ratios measured in tests of the planktic foraminifer *Trilobatus trilobus*. Our SST record reveals a 3.2 °C decrease from 7.4 to 5.8 Ma, significantly increasing previous estimates of late Miocene tropical cooling. Analysis of orbital-scale variability shows that before the onset of cooling, SST variations were dominated by precession-band (19-23 kyr) variability, whereas tropical temperature became highly sensitive to obliquity (41 kyr) after 7.5 Ma, suggesting an increase in high latitude forcing. We compare a revised global SST database with new paleoclimate model simulations and show that a $pCO_2$ decrease from 560 ppm to 300 ppm, in the range suggested by $pCO_2$ proxy records, could explain most of the late Miocene sea surface cooling observed at Site U1443. Using our new Site U1443 record as representative of tropical SST evolution, estimated meridional SST gradients suggest a much more modest increase over the late Miocene than previously suggested, in agreement with modelled meridional SST gradients.

## Plain Language Summary

The late Miocene is an interesting time period for paleoclimatologists because the Earth underwent important climatic and ecological changes that led to the establishment of our modern climate. An important cooling of global surface oceans was recorded by tracers used to reconstruct past temperature, however the amplitude of this cooling in the tropics and the role of atmospheric carbon dioxide ($CO_2$) in driving it are unclear. We present a new reconstruction of sea surface temperatures from the eastern equatorial Indian Ocean based on the temperature-dependent ratio of magnesium to calcium measured in fossil shells of zooplankton (Foraminifera). Our results reveal a cooling (3.2 °C) higher than previous estimates of tropical ocean cooling (1 to 2.5 °C). To understand the role of atmospheric $CO_2$ in driving this cooling

we simulated Miocene climate using a complex model, and find that an atmospheric $CO_2$ decrease from 560 ppm to 300 ppm could explain most of the reconstructed surface ocean cooling. We also find that ocean surface temperature gradient between the tropics (using our new reconstruction) and the northern high latitudes shows a more modest increase over the late Miocene than suggested by previous studies, in agreement with new and existing climate model results.

## 1 Introduction

The late Miocene (11.6 to 5.3 million years ago, Ma) lies in a context of long-term Cenozoic global cooling and declining partial pressures of atmospheric $CO_2$ ($pCO_2$) (Beerling & Royer, 2011; Westerhold et al., 2020; Rae et al., 2021), and offers the opportunity to assess the sensitivity of Earth's climate system to changing internal and external drivers in a warmer world with a continental configuration similar to modern (Knorr et al., 2011; Herbert et al., 2016; Holbourn et al., 2018; Steinthorsdottir et al., 2021). During the late Miocene, major global sea surface cooling is recorded in mid- and high-latitude sites in both hemispheres despite the absence of a strong trend in deep-ocean foraminiferal $\delta^{18}O$ that might imply sustained global cooling (Herbert et al., 2016; Westerhold et al., 2020). This occurs alongside major ecological events and carbon cycle shifts recorded both on land and in the oceans (e.g., Pound et al., 2012; Zhang et al., 2014; Bolton & Stoll 2013; Bolton et al 2016; Keigwin, 1979; Keigwin & Shackleton, 1980; Holbourn et al., 2018; Drury et al., 2021).

The diachronous rise to dominance of C4 grassland biomes in tropical and subtropical regions on land between 10 and 3.5 Ma is suggested to have been driven by aridification and/or a decrease in $pCO_2$, although additional regional drivers were likely important (Cerling et al., 1997; Pagani et al., 1999; Herbert et al., 2016; Andrae et al., 2018; Carrapa et al., 2019; Tauxe & Feakins, 2020). Although large-scale northern hemisphere glaciation did not occur until the latest Pliocene ~2.7 Ma (e.g. Balco & Rovey 2010; Bailey et al., 2012; Mudelsee & Raymo, 2005), episodic occurrences of ice rafted debris between 7 and 5 Ma in North Atlantic (Larsen et al, 1994; John & Krissek, 2002) and North Pacific (Krissek, 1995) sediments associated with positive benthic foraminiferal $\delta^{18}O$ excursions suggest the presence of small ephemeral ice sheets in Greenland and Alaska at this time (Hodell et al., 2001; Holbourn et al., 2018; Jöhnck et

al., 2020). The hypothesis that significant changes in the cryosphere occurred during the late Miocene, including the presence of northern hemisphere ice sheets, is supported by the dominant obliquity influence on global climate cycles after ~7.7 Ma, suggesting amplified high-latitude forcing (Drury et al., 2017; Drury et al 2021; Holbourn et al., 2018; Westerhold et al., 2020).

These studies collectively suggest that profound changes in climate, cryosphere, vegetation, and carbon cycle dynamics occurred in the late Miocene, yet the role of $pCO_2$ as a potential driver, in particular of global cooling, is unclear. Existing $pCO_2$ reconstructions are generally low-resolution, with some studies showing no major $pCO_2$ decrease during the late Miocene (e.g. Kürschner et al 1996; Pagani et al., 1999, 2005; Retallack 2009; Zhang et al., 2013), and others either directly (Bolton et al., 2016; Mejia et al., 2017; Stoll et al 2019; Tanner et al., 2020; Rae et al., 2021; Brown et al., 2022) or indirectly (Bolton & Stoll, 2013) suggesting that $pCO_2$ gradually decreased.

A recent study of sea surface temperatures (SSTs) reconstructed using the $C_{37}$ alkenone unsaturation index ($U^{k'}_{37}$ index) revealed global cooling from 7.5 to 5.5 Ma (termed the Late Miocene Global Cooling, LMCG), with a magnitude of 3 to 5 °C in high and mid-latitudes and a modest cooling of ~1 °C in the tropics (Herbert et al., 2016). While the linear relation between the $U^{k'}_{37}$ index and temperature is well defined for temperatures between 8 and 24 °C, it contains larger uncertainties at warmer temperatures (> 24 °C) due to a decrease in $U^{k'}_{37}$ sensitivity to temperature (e.g. Sonzogni et al 1998; Conte et al., 1998; Grimalt et al., 2001; Pelejero & Calvo, 2003; Conte et al., 2006; Tierney & Tingley, 2018). Thus, it is likely that tropical SSTs prior to the LMGC as well as the long-term amplitude of cooling recorded by the $U^{k'}_{37}$ index are underestimated (Herbert et al., 2016). Several low-resolution tropical Pacific temperature records based on the $TEX_{86}$ index also span the late Miocene, showing 2 to 4 °C of cooling (Zhang et al., 2014; Liu et al., Liu et al., 2020). SST estimates based on planktic foraminiferal Mg/Ca ratios from the South China Sea (Steinke et al., 2010; Holbourn et al., 2018) also suggest 2.5 °C of late Miocene cooling. A subtropical Mg/Ca-SST record from Southwest Pacific Deep Sea Drilling Project Site 590 (latitude ~31° S) spanning ~2.7 to 6.2 Ma is also available (Karas et al., 2011), however this record does not cover the LMGC interval and its interpretation is controvertial because of a possible change in upwelling regime with implications for the interpretation of the Mg/Ca signal (Dickens & Backman, 2012). Overall, existing late Miocene tropical SST records

are either from upwelling areas (Arabian Sea, Equatorial Pacific; Huang et al., 2007; Rousselle et al, 2013; Zhang et al., 2014; Herbert et al., 2016), or from regions affected by complex local oceanography (South China Sea and Andaman Sea; Holbourn et al., 2018; Jöhnck et al., 2020), precluding the resolution of globally representative tropical SST trends.

Here, we aim to better constrain the magnitude of tropical late Miocene cooling by reconstructing SSTs in an open-ocean, warm-pool region using a proxy that is well-suited to warm environments. We present new orbital-resolution SST estimates from sediments deposited at International Ocean Discovery Program (IODP) Site U1443, in the eastern equatorial Indian Ocean, spanning the late Miocene and earliest Pliocene (9 to 5 Ma). SSTs are estimated using Mg/Ca ratios measured in tests of the mixed layer dwelling foraminiferal species *Trilobatus trilobus*. To test the hypothesis that a $p\text{CO}_2$ decrease drove global sea surface cooling during the late Miocene, as suggested by recent studies (e.g., Herbert et al., 2016; Tanner et al., 2020; Rae et al., 2021), we present new climate model simulations using the Earth System Model IPSL-CM5A2 (Sepulchre et al., 2020). We evaluate the effect of $p\text{CO}_2$ on tropical SSTs and latitudinal SST gradients using three different $p\text{CO}_2$ scenarios within the range suggested by late Miocene $p\text{CO}_2$ proxy data (300, 420 and 560 ppm), and compare modelled SSTs to our new Site U1443 record as well as a revised global late Miocene SST data compilation.

## 2 Site Description and modern oceanography

IODP Site U1443 is located in the southernmost Bay of Bengal (BOB) and was cored during Expedition 353 on the crest of the Ninetyeast Ridge (5° 23' 2.94'' N, 90° 21' 40.381'' E, 2924 meters water depth) (Clemens et al., 2016). Site U1443 is a re-drill of Ocean Drilling Program (ODP) Site 758 (Shipboard Scientific Party, 1989). Due to the northward displacement of the Indian Plate, Site U1443 was located at a paleolatitude of 2.7°N at 9 Ma and 4°N at 5 Ma (Scotese, 2016).

In the modern northern Indian Ocean, seasonal South Asian monsoon circulation patterns are the dominant control on oceanographic conditions (Webster et al., 1998). Seasonal variations of insolation and pressure gradients between the southern subtropical Indian Ocean and the Asian continent induce a large-scale shift in surface wind direction and speed with strong

southwesterlies during the summer monsoon (June, July, August) and weaker northeasterlies during the winter monsoon (December, January, February) over the BOB (Tomczak & Godfrey, 2001). The BOB is also marked by a complete seasonal reversal of surface ocean circulation (Schott et al., 2009), with saltier, denser water masses from the Arabian Sea entering the BOB via the Southwest Monsoon Current during summer and less saline water masses from the BOB flowing into the Arabian Sea via the Northeast Monsoon Current during winter (Jensen, 2001 and 2003) (Figure 1a-b). In addition, the BOB receives a large amount of freshwater from direct rainfall and riverine inputs. This large input of freshwater and its redistribution by horizontal advection lead to the formation of strong salinity stratification governed by the seasonal and spatial variability of the barrier layer thickness (Shetye et al., 1996; Thadathil et al., 2007). The formation of a barrier layer between the base of the mixed layer and the top of the thermocline inhibits interactions between shallow and intermediate water masses, allowing BOB surface waters to maintain warm temperatures (>28 °C) throughout the year (Rao & Sivakumar, 2003; Thadathil et al., 2007). As a consequence, seasonal SST variability in the BOB is mainly controlled by the strength of (monsoonal) wind-driven mixing (e.g. Unger et al., 2003; Vidya et al., 2013) and by salinity stratification (barrier layer formation). In waters overlying Site U1443, strong southwesterlies result in maximum annual surface ocean wind stress, deeper wind-driven mixing and reduced stratification during the summer monsoon (Figure 1c). The intrusion of high salinity Arabian Sea water during summer also acts to deepen the mixed layer (Thadathil et al., 2007), resulting in average SSTs of 28.7 °C (Figure 1c), very close to mean annual SST (28.8 °C). In autumn and early winter, the progressive southward spreading of fresh water from riverine inputs in the northern BOB results in the development of salinity stratification and a barrier layer (Thadathil et al., 2007) and allows relatively warm SSTs (> 28.1 °C; Figure 1c) to persist above Site U1443. During this time the lowest sea surface salinities occur (33.6 to 33.8 PSU; Zweng et al., 2018), although the annual sea surface salinity range is small (33.6 to 34.35 PSU; Figure 1c) compared to further north in the BOB. SSTs reach a maximum of 29.9 °C in April, when lowest surface ocean wind stress results in strong stratification and a shoaling of the mixed layer (Figure 1c). In summary, local ocean-atmosphere processes induce a relatively small annual SST variability in waters overlying Site U1443 (28.1-29.9 °C; Figure 1c; Locarnini et al., 2018), thus we consider this site suitable for reconstructing "open ocean" tropical SSTs that are representative of the global picture.

# 3 Materials and Methods

## 3.1 Sampling and *Trilobatus trilobus* taxonomy and ecology

Site U1443 samples used in this study are from the revised shipboard splice comprised between 122.6 m and 70.06 m CCSF-A (Core Composite depth below Sea Floor), from Core U1443B-7H-5W to Core U1443C-15H-4W, spanning the late Miocene and earliest Pliocene (9 to 5 Ma) (Bolton et al., 2022). 1 cm thick half-rounds were sampled from the core working halves. Bulk samples were washed through a 63 μm sieve with tap water, then the coarse fraction was oven dried at 50 °C. Sediments are dominated by calcareous nannofossil ooze with well-preserved shell of foraminifera (~70-80 % $CaCO_3$ with slightly increasing clay content upcore) (Clemens et al., 2016). A detailed analysis of carbonate content and biogenic sediment mass accumulation for the same late Miocene splice interval is presented in Bolton et al. (2022). We apply the age model of Bolton et al. (2022), based on revised biostratigraphy and tuning of benthic foraminiferal $\delta^{18}O$ to an eccentricity-tilt target, which results in sedimentation rates between 0.5 and 1.9 cm/kyr. We selected 735 samples over the 9 to 5 Ma interval for Mg/Ca SST reconstruction, with a mean resolution of 5.5 kyr.

In each sample 50 to 60 tests of *Trilobatus trilobus* (Reuss, 1850) were picked from the 212-315 μm size fraction, avoiding individuals with gametogenic calcite that could introduce a cold bias due to migration during gametogenesis (Bé, 1980; Hemleben et al., 2012). In the modern ocean, *T. trilobus* is considered to be one of four morphospecies of the *Trilobatus sacculifer* plexus (Spezzaferri et al., 2015; Poole & Wade 2019). It ranges stratigraphically from the lower Miocene to recent (Spezzaferri 1994) and is very abundant in the tropical to subtropical oceans (Bé & Tolderlund, 1971; Schiebel & Hemleben, 2017). *T. trilobus* is a spinose, photosymbiont-bearing species that is therefore constrained to the upper photic zone, calcifying in the mixed layer, with low seasonality in stratified tropical waters (Schiebel & Hemleben, 2017). *T. trilobus* tests were abundant and well preserved throughout the late Miocene at Site U1443 (see section 4.1).

### 3.2 Mg/Ca-SST reconstruction

### 3.2.1 Mg/Ca Cleaning and Analysis

*Trilobatus trilobus* tests were weighed, gently crushed between two glass slides to open chambers, then fragments were homogenized before cleaning. Test fragments were cleaned to remove clay and organic matter, following the short "Mg cleaning" protocol of Barker et al. (2003) without a reductive step. A cleaning test was performed on ten samples throughout the study interval to test the sensitivity of measured Mg/Ca ratios to the inclusion of a reductive cleaning step (Rosenthal et al., 2004) (Text S1 and Figure S1). Samples were dissolved in 0.075 M $HNO_3$ and centrifuged to remove potentially remaining detrital particles (Greaves et al., 2005), then the solution was diluted with 2 % $HNO_3$. Samples were analyzed using bracketing to minimize instrumental drift with an ICP-QMS (Agilent 7500ce) at CEREGE. Together with Mg/Ca and Sr/Ca ratios, Fe, Al and Mn concentrations were analyzed. Long term precision determined by analysis of independent in-house standards during each run over 2 years is on average 0.56 % (r.s.d) for Mg/Ca. In nine samples, *T. trilobus* tests were also picked from the 355-500 μm size fraction and analyzed following identical protocols described above to access the sensitivity of Mg/Ca to test size (Text S2 and Figure S2).

### 3.2.2 Calibration

We compare SSTs reconstructed using three different *T. sacculifer* exponential calibration equations: the commonly-applied Anand et al. (2003) sediment trap calibration from the Sargasso Sea ("Mg cleaning", test size: 350-500 μm), the Dekens et al. (2002) calibration based on core top data from the tropical Pacific Ocean, which includes a basin-specific dissolution correction ("Cd cleaning", test size: 250-350 μm), and the Hollstein et al. (2017) calibration based on Western Pacific Warm Pool core-top data ("Cd cleaning", test size: 250-355 μm) (Figure S3). Because we find no systematic bias of Mg/Ca ratio according to cleaning method and test size (Texts S1-2 and Figures S1-2), we select the Dekens et al. (2002) calibration (Equation 1).

$$Mg/Ca = 0.37. \exp^{0.09[T-0.36(\text{core depth km})-2.0°C]} \qquad (1)$$

Core-top *T. trilobus* Mg/Ca ratios were estimated from *Globigerinoides ruber* Mg/Ca ratios measured in four core-top samples of Holocene age from Site ODP 758 ((Mg/Ca)$_{T.\ trilobus}$ = 3.74 ± 0.19 to 3.79 ± 0.19 mmol/mol), and yield reconstructed SSTs of 28.2 to 29.5 °C with Dekens et al. (2002) calibration, consistent with the modern mean annual SST range above the site (28.1 to 29.9 °C) (see Text S3, Table S1 and Figure S4 for detail about estimation of core-top *T. trilobus* Mg/Ca ratios based on Mg/Ca ratios measured in both *G. ruber* and *T.trilobus* in 50 samples from IODP Site U1443). In contrast, the Anand et al. (2003) calibration produces much cooler temperatures of 25.8 to 26.5 °C and the Hollstein et al. (2017) calibration produces slightly cooler temperatures of 27.8 to 29 °C when applied to core-top Mg/Ca values. The choice of calibration does not affect reconstructed SST trends (Figure S3).

### 3.2.3 Correction for Mg/Ca$_{sw}$

The residence times of Ca (~1.1 million years) and Mg (~13 million years) in the ocean (Broecker & Peng, 1982) suggest that Mg/Ca of seawater (Mg/Ca$_{sw}$) in the late Miocene may have been significantly different to the present-day value of 5.2 mmol/mol (Evans & Muller 2012). Thus, for reconstructions older than 1.1 Ma, it is necessary to correct Mg/Ca measured in foraminiferal tests for the effect of secular variations in Mg/Ca$_{sw}$ (e.g. Evans & Muller, 2012; Tierney et al. 2019). Cenozoic reconstructions of Mg/Ca$_{sw}$ are based on a variety of proxies including fluid inclusions in halite (Horita et al., 2002; Lowenstein et al., 2001), calcium carbonate veins (Coggon et al., 2010), benthic foraminifera (Lear et al., 2000), echinoderms (Dickson, 2002) and corals (Gothmann et al., 2015). However, the history of Mg/Ca$_{sw}$ is still poorly constrained by proxies, in particular for the late Miocene where data are sparse, and various modelling scenarios have also been proposed (Figure S5). We compared modelling scenarios and selected the HS15 scenario (Higgins & Schrag, 2015) based on pore fluid chemistry modelling for Mg/Ca$_{sw}$ correction in this study (see Text S4 for rationale). The effect of Mg/Ca$_{sw}$ variations on Mg/Ca$_{test}$ was corrected following the approach of Tierney et al. (2019)

with a linear relationship with H=1 instead of a power law relationship (Evans & Muller, 2012). Both of these Mg/Ca$_{sw}$-Mg/Ca$_{test}$ relationships are based on the same data derived from the *T. sacculifer* culture experiment in Delaney et al., (1985), thus we prefer to use the linear relation as it provides a simpler approach.

$$Mg/Ca_{test}^{t=t} = \frac{Mg/Ca_{sw}^{t=t\ H}}{Mg/Ca_{sw}^{t=0\ H}} \times B.exp^{AT} \qquad (2)$$

In Text S5, we discuss the effect of different H values and the impact of Mg/Ca$_{sw}$ correction on reconstructed SSTs.

### 3.3 Error propagation and time series analyses

Propagated Mg/Ca-SST ±1σ and 2σ uncertainties linked to analytical and age model errors were estimated via a bootstrap Monte Carlo procedure using the Paleo-Seawater Uncertainty Solver (PSU Solver; Thirumalai et al., 2016) in Matlab. The age model uncertainty used is 20 kyr and the average analytical uncertainty for Mg/Ca data is 0.02 mmol/mol. Uncertainties related to Mg/Ca$_{sw}$ are not included in the error propagation, and different scenarios are shown in Figure S6. 10 000 Monte Carlo iterations were performed.

Time series analyses were performed using the software package Acycle (Li et al., 2019) and cross-wavelet analyses were performed in R using the biwavelet package (Grinsted et al., 2004; Gouhier et al., 2016), on records resampled at constant 2 kyr intervals to preserve maximum resolution, and filtered to remove periodicities longer than one third of dataset length (>1.3 Ma). Evolutive and singular spectral analyses were performed with the Fast Fourier transform (LAH) method (Kodama & Hinnov, 2014) and the Multi Taper Method (Thomson, 1982), respectively. For evolutive analyses of Mg/Ca from Site U1443 a window of 800 kyr and a step of 100 kyr were used. Where records overlap (~8 to 5 Ma), our Site U1443 Mg/Ca record was compared to the South China Sea ODP Site 1146 Mg/Ca record (Holbourn et al., 2018), and LAH was performed with a window of 600 kyr and a step of 100 kyr. Cross-wavelet analyses were performed on Mg/Ca and benthic δ$^{18}$O records from site U1443, both records were resampled and filtered as described above.

### 3.4 Late Miocene SST modelling and data compilation

To simulate the effect of late Miocene $p$CO$_2$ decrease on tropical Indian Ocean SSTs we used the Earth System Model IPSL-CM5A2 (Sepulchre et al., 2020) that simulates the interactions between ocean, atmosphere, land and ice. The IPSL-CM5A2 coupled model is a combination of the LMDZ5A atmospheric model (Hourdin et al., 2013), the ORCHIDEE land surface model (Krinner et al., 2005) and the NEMOv3.6 oceanic model (Madec, 2016) that includes an ocean dynamic component (OPA; Madec, 2008), a sea-ice thermodynamics model (LIM2; Fichefet & Maqueda, 1997; Timmermann et al., 2005) and a biogeochemistry model (PISCES-v2; Aumont et al., 2015). The ocean component has a horizontal resolution of 2° by 2° (refined to 0.5° in the tropics) and 31 vertical levels, whose thickness increases from 10 m at the surface to 500 m at the bottom. The atmospheric component has a horizontal resolution of 1.875° in latitude by 3.75° in longitude with 39 vertical levels. The ocean-atmosphere coupling is ensured by the OASIS3-MCT 2.0 coupler (Valcke, 2013) that interpolates and exchanges variables between the two components.

Vegetation in the model is prescribed by latitudinal band (as in Sarr et al., 2022). The modelling framework we use does not include a dynamic vegetation model and we do not account for Miocene vegetation distribution. We are aware of the potential effect on surface temperature that can be induced by considering appropriate vegetation cover, for example Micheels et al. (2007) simulated a 0.9°C global temperature increase when a Tortonian vegetation reconstruction was applied compared to present day vegetation, although the largest changes occurred in continental regions. In addition, the late Miocene time interval studied encompasses the transition from C3 to C4 plants, which likely resulted in vegetation changes that affected surface properties and potentially on the Δtemperature that we simulated between our different model simulations. Burls et al. (2021) estimated the model sensitivity (i.e., the mean global temperature response to a $p$CO$_2$ doubling) of the IPSL-CM5A2 model to be >4°C, based on middle Miocene climate simulations with 2x and 4x pre-industrial $p$CO$_2$. This updated version thus has a slightly higher model sensitivity than IPSL-CM5A (Dufresne et al. 2013; 3.6°C) but remain in the range of

CMIP5 model sensitivity. Burls et al. (2021) indeed obtained a mean sensitivity of ~3.92°C in the framework of a multi-model inter-comparison for the Miocene.

We used the late Miocene paleogeography from Sarr et al. (2022) that is based on PLIOMIP (Haywood et al., 2020) with additional manual modifications. Those include a more exposed Sundaland and the Australian continent located further south relative to its modern position, which result in a wider Indonesian Gateway that connects West Pacific and tropical Indian Ocean water masses via Indonesian Throughflow (ITF). Other differences include a closed Bering Strait and the absence of Hudson Bay. A small ice-sheet is present on Greenland and the size of the Antarctic Ice Sheet is reduced compare to present-day, with the removal of the West Antarctic ice sheet. Given the range of $p$CO$_2$ reconstructed by various proxies for the late Miocene (1 to 3 times pre-industrial values of 280 ppm, see section 5.2, Table S2), we designed three simulations with atmospheric $p$CO$_2$ values of 300, 420 and 560 ppm respectively. The solar constant was set at 1364.3 W.m$^{-2}$ and orbital parameters were kept at modern values.

To enable comparison between existing SST records and our new Indian Ocean record, as well as a model-data comparison, we compiled all available late Miocene Mg/Ca, U$^{k'}_{37}$, and TEX$_{86}$ data (Table S3) and recalculated SSTs using consistent calibrations and corrections. Mg/Ca-SSTs (Holbourn et al., 2018; Jöhnck et al., 2020) were recalculated using the Dekens et al. (2002) calibration and a Mg/Ca$_{sw}$ correction as described in Section 3.2. U$^{K'}_{37}$-SSTs (Huang et al., 2007; Rommerskirchen et al., 2011; LaRiviere et al., 2012; Rousselle et al., 2012; Seki et al., 2012; Zhang et al., 2014; Herbert et al., 2016; Liu et al., 2019) were recalculated using the BAYSPLINE calibration to account for the attenuation of the U$^{k'}_{37}$ responses to SST at temperatures >24 °C (Tierney & Tingley, 2018). TEX$_{86}$-SSTs (Zhang et al., 2014; Super et al., 2020) were recalculated using the BAYSPAR calibration analog mode (Tierney & Tingley, 2015). We then compared our revised global SST compilation, averaged over two one-million-year time windows centred on 8 and 6 Ma, to modelled latitudinal SST gradients. We chose these time windows to represent SSTs before and after the LMGC while excluding the effect of short term/orbital-scale variability, and to investigate the potential role of $p$CO$_2$ in driving this long-term cooling. To calculate the paleopositions at 6 and 8 Ma for each site, we used GPlates

software (http://www.gplates.org), using rotations and plate boundaries from the PALEOMAP PaleoAtlas for Gplates (Scotese, 2016).

## 4 Results

### 4.1 Validity of Mg/Ca$_{foram}$ for SST reconstruction at Site U1443

Indicators of cleaning performance and test dissolution suggest that our Mg/Ca record is suitable for SST reconstruction (Figure S7). Fe/Ca, Al/Ca and Mn/Ca show no correlation with Mg/Ca (Figure S7a-c), suggesting that the influence of clay minerals and manganese oxides on foraminiferal Mg/Ca is negligible. Test dissolution preferentially removes Mg (Brown & Elderfield, 1996; Lea et al., 1999; Rosenthal et al., 2000; Dekens et al., 2002) and lowers foraminiferal test weight (Rosenthal & Lohman, 2002; Lea et al., 2006) and the percentage of coarse fraction (Bassinot et al., 1994). It is also possible that foraminiferal Sr/Ca decreases as carbonate dissolution advances (Stoll et al., 1999). We find no correlation between Mg/Ca ratio and Sr/Ca, mean mass of individual tests, or % coarse fraction (Figure S7d-f), which gives us confidence that dissolution is unlikely to have influenced temporal variations in Mg/Ca. Scanning Electron Microscope (SEM) images of *T. trilobus* tests in selected samples also attest to their good preservation (Figure S7). Tests are devoid of secondary inorganic calcite crystals on their surface and inner walls, easily identifiable at the micron scale (Edgar et al., 2015; Sexton et al., 2006), and the pore structure appears well preserved. Cross-section images of test walls show a microgranular texture without secondary calcite crystals, suggesting that the initial biogenic structure of the test is preserved.

In certain regions, strong seasonality in planktic foraminiferal production and shell flux can bias Mg/Ca SST records away from mean annual values (e.g. Jonkers et al., 2010, 2013). In the region of Site U1443, annual SST variability is small (~1.7 °C), and two productivity maxima occur over the annual cycle. The largest primary productivity peak occurs during late summer (July, August, September; mean SST 28.5 °C) and a second peak is observed in winter (December, January, February; mean SST 28.6 °C) (Rixen et al., 2019). The seasonality of planktonic foraminiferal mass fluxes recorded at a southern Bay of Bengal sediment trap site

seems to broadly follow annual primary productivity and are highest during July, September and January (Ramaswamy & Gaye, 2006). Thus, even if foraminiferal shell fluxes were biased towards high productivity seasons, temperatures recorded by *T. trilobus* at Site U1443 are still representative of mean annual mixed-layer temperatures (28.8 °C), with a possible small bias towards cooler SSTs (less than −0.3 °C).

Some studies have demonstrated that planktic foraminiferal Mg/Ca can be highly sensitive to salinity and pH changes in some species (Mathien-Blard & Bassinot, 2009; Allen et al., 2016; Gray & Evans 2019). Above Site U1443, modern sea surface salinity is close to the open-ocean value of ~34 PSU and seasonal variations are small (< 1 PSU). Tierney et al. (2019) suggest that SST sensitivity to salinity is low between 33 and 38 PSU. Thus, we consider a monsoon-related salinity influence on Mg/Ca at this site to be unlikely. Similarly, only small long-term changes in benthic $\delta^{18}O$ are recorded at Site U1443 and these are independent in timing from SST trends (Figure 2), suggesting no large influence of global sea level-related salinity changes on Mg/Ca. In Text S6 we discuss in detail the sources of potential salinity variation above Site U1443 and evaluate the salinity influence on Mg/Ca-SST by combining the equations by Gray & Evans (2019) and Dekens et al. (2002). In cultures of *T. sacculifer,* no pH effect on Mg/Ca is detected (Allen et al., 2016; Gray & Evans 2019), thus, calibration equations do not include a term to correct for the pH effect (Gray & Evans, 2019; Tierney et al. 2019). In addition, Site U1443 paleoproductivity and biogenic sedimentation records suggest that this site was insulated from large long-term changes in productivity over the late Miocene (Bolton et al., 2022), suggesting that temporal changes in pH related to upwelling are unlikely to have occurred. In summary, Mg/Ca ratios measured in *T. trilobus* are interpreted as representative of past mean annual temperatures in the upper mixed layer of the ocean above Site U1443, with negligible influence of salinity or pH.

## 4.2 Orbital-scale SST variability

Late Miocene SSTs at Site U1443 show significant (up to 3 °C amplitude) orbital-scale variability, which is unaffected by Mg/Ca$_{sw}$ correction. During certain Thvera-Gilbert (TG) cold stages (Shackleton et al., 1995) recorded in benthic oxygen isotopes from the same site (Bolton et al., 2022), coolings of 0.7 to 2.3 °C are recorded (Figure 2). We note that the relatively low

sedimentation rates at Site U1443 of on average between 1 and 1.7 cm kyr$^{-1}$ during the study interval (Bolton et al., 2022) mean that bioturbation has likely smoothed or reduced the amplitude of orbital-scale (and in particular precession-scale) variability in our SST record. The Mg/Ca record is characterized by >99 % significant variability at the orbital periods 41 kyr, 24 kyr and 20 kyr, and at the non-primary orbital periods 49 and 59 kyr (Figure 3). At the onset of the LMGC around 7.7 to 7.5 Ma, 41 kyr and 49 kyr cycles emerge (Figure 3c), and before 7.5 Ma precession-band variability (24 and 20 kyr) is more pronounced (Figure 3d). Evolutive spectral analysis of the Mg/Ca record also shows variability at the ~400 kyr (Figure 3b) period, but this period is only >95 % significant in the interval before 7.5 Ma (Figure 3d). Pronounced periods at 225 and 231 kyr (> 99 % significant) are also identified in the Mg/Ca spectrum, and two well-defined ~200 kyr cycles are visible between 9 and 8.6 Ma (Figures 2-5).

## 4.3 Long term SST trends at Site U1443

Mg/Ca shows a slightly increasing trend from 9 to 7.4 Ma, with values comprised between 3.90 and 2.67 mmol/mol (mean = 3.24 mmol/mol, $n$ = 345, SD = 0.45 °C; Figure 2a). Mg/Ca ratios then decrease between 7.4 and 5.8 Ma by 0.55 mmol/mol, reaching a minimum average value of 2.81 mmol/mol between 6.2 and 5.8 Ma (Figure 2a). Values then increase from 5.8 to 5 Ma by 0.2 mmol/mol. Reconstructed SSTs (uncorrected and corrected for Mg/Ca$_{sw}$ variations) show the same long-term trends and structure as raw Mg/Ca data, with higher SSTs in the oldest part of the record, a long-term gradual cooling from 7.4 to 5.8 Ma, an SST minimum at 5.8 Ma followed by a warming between 5.8 and 5 Ma (Figure 2a). With no Mg/Ca$_{sw}$ correction, calculated SSTs over the whole record vary between 23.7 °C and 29.2 °C with a mean value of 26.7 °C (Figure 2a, blue curve). Application of our preferred correction for secular changes in Mg/Ca$_{sw}$ (see Methods, Texts S3-4) increases absolute SST estimates by 2.5 to 4.9 °C relative to uncorrected SSTs, and increases the slope of reconstructed long-term cooling by 31 % (Figures 2a and S5). Corrected SSTs vary between 26.7 °C and 34.1 °C with a mean value of 30.4 °C *(n=735, SD= 1.35°C)*, and are above the modern and core-top range prior to 6.5 Ma and close to or within the modern range between 6.5 and 5 Ma (Figure 2a, red curve). The warmer temperatures from 9 to 7.4 Ma fluctuate between 29.6 °C and 34.1 °C with a mean of 31.6 °C *(n=345, SD 0.7 °C)*. This

warm period is followed by a gradual cooling of 3.2 °C from 7.4 to 5.8 Ma. From 5.8 Ma until ~5.4 Ma, SST increases by 1 °C.

## 5 Discussion

### 5.1 Drivers of tropical Indian Ocean SST variability on orbital timescales

Time series analyses of the Site U1443 late Miocene Mg/Ca record reveal a major increase in SST sensitivity to obliquity forcing around 7.5 Ma, at the onset of the LMGC (Figures 3b-d, S7). The appearance of the 49 kyr heterodyne (non-primary orbital period) after 7.5 Ma, alongside an increase in SST variability at the (near-primary) 40 kyr period, could result from the interference of obliquity (41 kyr) and precession (22.4 kyr) periods (Thomas et al., 2016). Before that, from 9 to 7.5 Ma, orbital scale SST variability was dominated by precession-band variance (Figure 3d). The influence of precession on tropical Indian Ocean SSTs can be explained either by its direct influence on the seasonal distribution of radiation (Clement et al., 2004), or by its influence on the strength of monsoon winds (e.g., Bosmans et al., 2018), which in turn affect mixed-layer depth and SST (Figure 1). Recent data indicate that no major long-term change in South Asian monsoon wind strength over the equatorial Indian Ocean occurred during the late Miocene (Betzler et al., 2016, 2018; Bolton et al., 2022), suggesting that an increase in wind-driven mixing is unlikely to have contributed to the increase in sensitivity of SST to orbital forcing that we document at Site U1443.

Obliquity cycles are also identified in the ODP Site 1146 Mg/Ca-SST record from the South China Sea, with a similar increase in power after 7.5 Ma (Figure S8; Holbourn et al., 2018). The direct effect of obliquity on low-latitude insolation is small, and the appearance of strong obliquity cycles in tropical SSTs is broadly concurrent with their appearance in benthic $\delta^{13}$C and $\delta^{18}$O from Site U1443 (Bolton et al., 2022) and in a late Miocene benthic $\delta^{18}$O global stack (Drury et al., 2021), suggesting an increase in tropical SST sensitivity to obliquity linked to an increase in high latitude forcing. Cross-wavelet analysis of SST and benthic $\delta^{18}$O from Site U1443 show high coherency (>95 %) in the obliquity band (Figure 3e), suggesting that SSTs and deep ocean $\delta^{18}$O (linked to continental ice volume and temperature in deep-water formation

regions) were coupled on orbital timescales during the late Miocene. A number of studies suggest significant changes in cryosphere dynamics during the late Miocene, with the development of ephemeral and dynamic Northern Hemisphere ice sheets (Larsen et al, 1994; Krissek, 1995; Hodell et al., 2001; John & Krissek, 2002; Holbourn et al., 2018; Miller et al. 2020) and Antarctic glacial expansion (Warnke et al., 1992; Ohneiser et al., 2015, Levy et al., 2019). One hypothesis to explain the increased sensitivity to obliquity recorded both in benthic foraminiferal isotopes and in tropical SSTs is that changes in cryosphere dynamics occurring during the LMGC rendered the Earth's climate system more sensitive to obliquity and that feedbacks associated with glacial-interglacial variability also started to affect tropical SSTs after ~7.5 Ma. For the last 0.8 million years, coherence in cyclicity between tropical SSTs and direct measurement of glacial-interglacial variations of atmospheric $CO_2$ and other greenhouse gases captured in ice cores (Petit et al., 1999; Spahni et al., 2005; Lüthi et al., 2008) support the hypothesis that radiative forcing by atmospheric $CO_2$ play a dominant role in modulating tropical SST variability on glacial-interglacial timescales (Visser et al. 2003; Lea, 2004; Past Interglacials Working Group of PAGES, 2016). At present, there are no late Miocene $p CO_2$ reconstructions with a sufficient resolution to allow direct comparison of SSTs and $p CO_2$ at the glacial-interglacial timescale. In the late Pliocene to early Pleistocene, after the onset of large-scale Northern Hemisphere glaciation at ~2.7 Ma, tropical SSTs are reported to exhibit strong variability on glacial-interglacial timescales, coeval with global climate cycles recorded in benthic $\delta^{18}O$ and $p CO_2$. Low-latitude SST records show a dominance of 41-kyr cycles before the mid-Pleistocene transition (occurring between 1.2 and 0.6 Ma) and the emergence of 100-kyr cycles during the late Pleistocene (e.g. Liu & Herbert 2004; Liu et al., 2008; Herbert et al., 2010; Li et al., 2011; Li et al., 2017), suggesting "top-down" forcing of tropical SSTs via greenhouse gas forcing. Our late Miocene SST data, considered alongside data from South China Sea Site 1143 (Holbourn et al., 2018), suggest that tropical SSTs became more tightly coupled to glacial-interglacial climate and $p CO_2$ cycles after ~7.5 Ma.

In addition to variability in the obliquity and precession bands, our Mg/Ca-based SST record show variability at the ~400 kyr period (Figure 3b and d; 95 % coherency), which could result from the direct influence of long eccentricity cycles or the modulation of precession by

eccentricity. A number of other studies have recorded ~400 kyr cyclicity in Plio-Pleistocene tropical SSTs (Gupta et al., 1996; Lawrence et al., 2006; Herbert et al, 2010; Li et al, 2011; Li et al., 2017), but the mechanisms involved remain unclear. In one study from the South China Sea, ~400-kyr cycles in SST were suggested to be related to the modulation of the East Asian winter monsoon by El Nino-Southern Oscillation (Li et al., 2017). The presence of ~225 kyr cycles, with two well-defined cycles visible in the oldest part of the Site U1443 SST record between 9 and 8.6 Ma (Figures 2-5) could either represent a real cycle in eccentricity (Hilgen et al., 2020) or a harmonic of the influence of long eccentricity cycles.

## 5.2 Late Miocene tropical sea surface cooling

Our new open-ocean tropical Indian Ocean SST record documents a late Miocene cooling of 3.2 °C starting at 7.4 Ma and culminating in minimum temperatures from 6.2 to 5.8 Ma. Following this, a warming of ~1 °C occurs from 5.8 to ~5.4 Ma (Figures 2, 4 and 5). We note that although absolute reconstructed SSTs and the magnitudes of change are sensitive to Mg/Ca$_{sw}$ and H value corrections, the magnitude of cooling from 7.4 to 5.8 Ma is above 2.5°C in all scenarios (Text S4, Figure S6). These broad trends and timings are coherent with stacked $U^{k'}_{37}$-SSTs, although Herbert et al. (2016) record tropical cooling not exceeding 1.5 °C (Figure 4a). SSTs in Eastern Equatorial Pacific (EEP) ODP Site 850 and in West Pacific Warm Pool (WPWP) ODP Site 806 reconstructed with the TEX$_{86}$ index (Zhang et al., 2014) record ~2 °C and 1.5 °C of cooling from 7.5 to 5 Ma, respectively, whereas TEX$_{86}$-SSTs at ODP Site 1143 in the South China Sea (Zhang et al., 2014) show a <1 °C cooling over the same period (Figure S9b). The three tropical sites where SSTs were reconstructed using *T. trilobus* Mg/Ca ratios (Figure 5a-c) show broadly similar long-term trends, although the amplitude of SST changes and exact timings are variable. The less pronounced late Miocene cooling trend in all $U^{k'}_{37}$ and some TEX$_{86}$ records compared to Mg/Ca-SSTs from Site U1443 may stem from proxy biases (discussed in section 5.2.1), aliasing due to the low resolution of many records, and/or errors related to the use of shipboard biostratigraphy and magnetostratigraphy for age control.

Late Miocene sea surface cooling at Site U1443 could be linked to a long-term increase in South Asian monsoon strength, because strong winds above Site U1443 during the summer monsoon deepen the mixed layer, increasing productivity and reducing SSTs (Fig. 1d). However, new high-resolution paleoproductivity records from the same Site U1443 sedimentary sequence suggest that South Asian monsoon winds were already established by 9 Ma in the equatorial sector of the Indian Ocean, with no apparent intensification over the late Miocene 9 to 5 Ma study interval. Thus, Site U1443 data do not suggest a long-term increase in export productivity (and inferred monsoon wind strength) that might have contributed to the SST cooling reconstructed from Mg/Ca ratios. A decoupling between productivity (related to monsoon wind strength) and SST (potentially linked to global climate) at Site U1443 during the late Miocene is further supported by the distinct orbital-scale variability of the records, with export productivity records showing dominant precession-scale variability (Bolton et al., 2022) and the SST record exhibiting dominant obliquity-scale variability (Fig. 3).

A driver of documented global sea surface cooling could be a decrease in $p$CO$_2$. Indeed, while certain late Miocene $p$CO$_2$ reconstructions based on carbon isotopic fractionation ($\delta^{13}$C) in alkenones (Pagani et al., 1999, 2005; Zhang et al., 2013), leaf stomata (Kürschner et al., 1996; Retallack, 2009; Stults et al 2011), and planktic foraminiferal boron isotopes ($\delta^{11}$B) (Sosdian et al., 2018) suggested relatively constant $p$CO$_2$ close to preindustrial values (~250-350 ppm), a number of recent studies that include higher-resolution sampling and/or new interpretive frameworks now point towards higher Miocene $p$CO$_2$ and a significant decrease over the late Miocene (Brown et al., 2022 ; Bolton et al., 2016; Mejia et al., 2017; Stoll et al 2019; Tanner et al., 2020; see also the review and revision of published $p$CO$_2$ data in Rae et al., 2021) (Table S2). For instance, studies based on marine phytoplankton $\delta^{13}$C suggest a $p$CO$_2$ decrease from between 800 and 560 ppm at 7.5 Ma to ~350 to 300 ppm at 5 Ma (Mejia et al., 2017, Tanner et al., 2020). Indirect evidence from the $\delta^{13}$C composition of coccoliths, arising about 7 to 5 Ma ago and interpreted as a threshold response of cells to decreasing aqueous CO$_2$ concentrations, also strengthens the hypothesis of declining $p$CO$_2$ during the late Miocene (Bolton & Stoll, 2013).

Therefore, considering a $p$CO$_2$ range in agreement with available proxy reconstructions (Figure 4b), we used late Miocene paleoclimate simulations under three atmospheric $p$CO$_2$ scenarios to test if a $p$CO$_2$ decrease may have driven global sea surface cooling over the late Miocene, and to estimate how much of the 3.2 °C tropical SST cooling observed at Site U1443 could be explained by $p$CO$_2$ forcing. In the following we compare compiled global SSTs at 8 ±0.5 Ma and at 6 ±0.5 Ma (see section 3.4) with SSTs simulated at 300 ppm (LM-300), 420 ppm (LM-420) and 560 ppm (LM-560) (Figures 6-7).

### 5.2.1 Tropical sea surface temperature records and model results

At 6 ±0.5 Ma, SSTs from the LM-300 simulation fit well with all tropical proxy-derived SSTs (Figure 6a), except two sites that show slightly warmer reconstructed SSTs compared to modelled ones at the same locations; ODP Sites 1146 (Holbourn et al., 2018) and 806 (Zhang et al., 2014) (site locations are shown in Figure 7). Site 1146 in the semi-enclosed South China Sea is under the influence of the East Asian monsoon subsystem, and the stepwise cooling in Mg/Ca-SSTs at 6.8 Ma (Figure 5b) has been attributed to a southward shift of the Intertropical Convergence Zone linked to cooling of the Northern Hemisphere and a consequent change in monsoon regime (Holbourn et al., 2018). At Site 806 in the WPWP, TEX$_{86}$-SSTs are above 28 °C for the entire record (Zhang et al., 2014), coherent with expected SSTs for warm pool regions (e.g. Vinayachandran & Shetye, 1991; Yan et al., 1992). However, Site 806 is thought to record the Miocene evolution of the proto-WPWP, forced by tectonic constriction of the Indonesian Gateway and eustatic fluctuations (Kuhnt et al., 2004; Sosdian & Lear, 2020), potentially affecting SST trends (e.g. Nathan & Leckie, 2009; Sosdian & Lear, 2020). Therefore, additional regional influences at these two sites could explain the discrepancies between modelled and reconstructed SSTs (Figure 6a). The LM-300 simulation also shows good agreement with SST data at 6 ±0.5 Ma in mid and high latitudes, except in the North Atlantic Ocean and one site in the South Pacific (Figure 6a). The discrepancy between proxy- and model-derived SSTs in the North Atlantic is a systematic bias in paleoclimate modelling studies (e.g. Dowsett et al., 2013; Burls et al. 2021) and is present in all our simulations (see section 5.2.3).

We next compared compiled SST data at 8 ±0.5 Ma to SSTs in LM-300, LM-420 and LM-560 simulations (Figure 6b). SSTs from the LM-300 simulations are too low compared to proxy-derived SSTs from all latitudes, with the exception of $TEX_{86}$-SSTs from the EEP cold tongue and from the South China Sea (Sites 850 and 1143, respectively, Zhang et al., 2014) . SSTs from the LM-560 and LM-420 simulations show good agreement with SST data at 8 ±0.5 Ma for mid and high latitudes (excluding the North Atlantic Ocean) but differ in the tropics. SSTs in LM-560 fit well with tropical Mg/Ca-SSTs from Site U1443 and $TEX_{86}$-SSTs from Site 806, but are warmer than tropical $U^{k'}_{37}$-SSTs (Figure 6b). Conversely, SSTs in the LM-420 simulation show better agreement with tropical $U^{k'}_{37}$-SSTs but are cooler than Site U1443 Mg/Ca-SST and Site 806 WPWP records (Figure 6b). $TEX_{86}$-SSTs from the EEP (Site 850) and the South China Sea (Site 1143) are cooler than in the LM-420 and LM-560 simulations.

A number of studies have demonstrated the limitations of alkenone paleothermometry for reconstructing SSTs in warm waters. The first concerns the application of a classical linear calibration (e.g. Prahl et al., 1988; Müller et al., 1998) that results in underestimation of temperatures >24 °C (e.g. Goni et al., 2001; Richey & Tierney, 2016). For this reason, we recalculated all $U^{k'}_{37}$-SSTs with the updated BAYSPLINE calibration (Tierney & Tingley, 2018). Another limitation concerns the difficulty of measuring very low concentrations of tri-unsaturated $C_{37}$ alkenones in sediments when the $U^{k'}_{37}$ index approaches its limit of 1, indicative of temperatures higher than 28 °C (Grimalt et al., 2001; Pelejero & Calvo, 2003; Richey & Tierney, 2016). Because of this, all published tropical $U^{k'}_{37}$-SST records come from sites located in upwelling regions. Arabian Sea ODP Site 722 is located in a coastal upwelling region forced by the southwest winds of the South Asian summer monsoon. Other sites (ODP Sites 846, 850, U1338 and 1241) are located in the EEP. Sites 846, 850 and U1338 are under the influence of cold tongue upwelling or equatorial divergence and Site 1241 is out of the upwelling centre today but was located further south, closer to the equatorial divergence, during the late Miocene (Mix, 2003). However, in all of these sites, in sediments older than 6.5 to 7 Ma, the $U^{k'}_{37}$ index approaches its limit of 1 ($U^{k'}_{37}$ = 0.96 to 0.99). This could provide an explanation for the lower tropical SSTs derived from the $U^{k'}_{37}$ index before 6.5 Ma, and therefore for the less pronounced tropical cooling in $U^{k'}_{37}$ records during the LMGC (on the order of 1-2 °C when recalculated with BAYSPLINE calibration; Figures 7 and S8a) compared to cooling from Mg/Ca-SST and

from modelled SST (Figures 6-7). Moreover, these upwelling systems in the EEP and Arabian Sea are dynamic and their strength depends both on oceanographic and paleogeographic constraints, with significant changes suggested for the Miocene (Holbourn et al., 2014; Tian et al., 2014; Zhang et al., 2014; Gupta et al. 2015; Zhuang et al. 2017; Bialik et al., 2020; Sarr et al. 2022). Thus, it is difficult to decouple the impact of changes in upwelling strength on SSTs from global SST trends at these sites.

$TEX_{86}$-SSTs reconstructed at ODP Site 850 (Zhang et al., 2014) record very variable temperatures from 9 to 5 Ma comprised between 21 and 32 °C with minimum temperatures between 5.5 and 5 Ma (21 to 23 °C), whereas $U^{k'}_{37}$-SSTs from the same site are less variable between 27.5 and 29 °C (Figure S9). In the modern ocean, ODP Site 850 is located in the EEP cold tongue, characterized by a shallow thermocline and intense upwelling. Lawrence et al. (2020) compared orbital-scale $TEX_{86}$ and $U^{k'}_{37}$ derived temperatures from ODP Site 846 in the EEP and showed that $TEX_{86}$ derived temperatures were consistently offset toward colder values with higher amplitude orbital-scale variability compared to $U^{k'}_{37}$ derived temperatures. This study proposes that the $TEX_{86}$ signal is also sensitive to local primary productivity, explaining the discrepancies observed between $TEX_{86}$ and $U^{k'}_{37}$ derived temperatures. One other plausible explanation for this discrepancy between $TEX_{86}$ and $U^{k'}_{37}$ temperatures could be that the $TEX_{86}$ paleothermometer records a depth-integrated signal rather than a surface one, as many studies have reported that GDGT producers can inhabit a large vertical range in the water column (e.g. Lipp & Hinrichs, 2009; Ho & Laepple, 2015, 2016; Richey & Tierney, 2016; Leduc et al., 2017; Van der Weijst et al., 2021). Given the potential underestimation of tropical $U^{k'}_{37}$-SST before ~6.5 Ma and the possibility that $TEX_{86}$ temperatures recorded at Sites 850 represent cooler subsurface waters, we think that the LM-560 scenario shows the best fit with SST data for 8 ±0.5 Ma.

### 5.2.2 $pCO_2$ as a primary driver of late Miocene cooling

In light of our data-model comparison, and considering our new tropical SST record and recent advances in $pCO_2$ estimates, we consider that the most likely scenario for late Miocene $pCO_2$

evolution is represented by an almost halving of $p$CO$_2$ during the LMGC (from 560 ppm around 8 Ma to 300 ppm around 6 Ma in our simulations, although absolute values remain uncertain). In the vicinity of Site U1443, simulated SSTs are 32 to 32.5 °C in the LM-560 simulation (interpreted as representative of ~8 Ma) and 29.5 to 30 °C in the LM-300 simulation (representative of ~6 Ma) (Figure S10) implying that 2 to 3 °C of sea surface cooling can be explained by atmospheric $p$CO$_2$ decrease and associated atmosphere-ocean feedbacks. This represent 63 to 94 % of the total late Miocene SST cooling (3.2 °C) estimated at Site U1443, corroborating the hypothesis that long-term SST evolution at this location is relatively insulated from local processes and is representative of global low-latitude trends over the late Miocene. Our new tropical SST record significantly increases previous estimates of tropical cooling during the late Miocene, with implications for estimates of climate sensitivity (to date based on tropical U$^{k'}_{37}$-SSTs; Brown et al., 2022) and the evolution of meridional thermal gradients (Herbert et al., 2016). Nevertheless, based on the results of our $p$CO$_2$ simulations, up to a third of the late Miocene cooling estimated for the equatorial Indian Ocean could be linked to other (presumably regional) phenomena, discussed below.

Extension of the Antarctic ice sheet during the late Miocene could have influenced water mass properties in deep-water formation regions, which in turn could have impacted low-latitude surface waters via plumbing to upwelling regions (Warnke et al., 1992; Ohneiser et al., 2015, Levy et al., 2019); however, this mechanism is unlikely to have contributed to SST cooling at Site U1443. On the other hand, regional tectonic activity (the collision of Australia and eastern Indonesia since the early Miocene, progressive constriction and shoaling of Indonesian Gateway), and glacio-eustatic sea level fluctuations that affected the geometry of the Indonesian Gateway and ITF (e.g. Kuhnt et al., 2004; Hall, 2009; Molnar & Cronin, 2015; Sosdian & Lear, 2020) could have influenced regional SSTs during the late Miocene. In the modern, warm, fresh waters flowing from the Pacific into the Indian Ocean via the ITF contribute significantly to intermediate water masses that occupy the Indian Ocean thermocline (You & Tomczak, 1993; Gordon & Fine, 1996; Tomczak & Godfrey, 2001; Gordon, 2005). Our late Miocene simulations do not account for any potential paleogeographic or ITF changes coeval with the LMGC, because the model resolution is insufficient to allow us to reconstruct the complex geography of the Indonesian Gateway area. Previous modelling studies however suggest that an ITF restriction

could generate a 2 to 3 °C cooling of surface and subsurface waters in the eastern Indian Ocean (Cane & Molnar 2001; Krebs et al., 2011). Although the exact timing of the gateway constriction is still poorly constrained, with estimates ranging from ~17 Ma to 4 to 3 Ma (e.g. Kennett et al., 1985; Hodell & Vayavananda, 1993; Hall et al, 1988, Hall, 2002,2012; Kuhnt et al.,2004; Li et al., 2006; Gallagher et al. 2009, Nathan & Leckie, 2009), late Miocene changes related to tectonic activity and/or sea-level drop linked to Antarctic glaciation remains one plausible mechanisms for amplification of cooling magnitude in the equatorial Indian Ocean (Site U1443). Additional late Miocene SST and other proxy records from the Australian Shelf and Timor Sea are needed to allow precise reconstruction of the timing of late Miocene ITF restriction, and to gain a better understanding of the effect of these changes on Indian Ocean SSTs.

### 5.2.3 Extratropical sea surface temperatures and late Miocene evolution of meridional gradients

In our data-model comparison, proxy-derived extratropical SSTs at 8 ±0.5 Ma and at 6 ±0.5 Ma show good agreement with modelled SSTs from our preferred scenario ($p$CO$_2$ decrease from 560 ppm to 300 ppm) both in term of absolute temperature and amplitude of cooling (Figures 6 and 7) except for the North Atlantic Ocean where proxy-derived SSTs are always warmer than modelled SSTs (Figure 6). This feature is a systematic bias in paleoclimate modelling studies that generally fail to reproduce estimated latitudinal temperature gradients (e.g. Dowsett et al., 2013; Burls et al., 2021). Temperature biases are often attributed to poor representation of cloud microphysics and/or to a lack of cloud-aerosol interaction in state-of the art climate models (Burls et al., 2021; Zhu et al., 2019), although Otto-Bliesner et al. (2017) also suggest that the failure to reproduce warm North Atlantic SSTs in Pliocene simulations (Dowsett et al. 2013) could be attributed to the inexact representation of Arctic gateways that are crucial for the simulation of Atlantic Meridional Overturning Circulation and North Atlantic climate sensitivity. In addition, Mejia et al. (2020) recently used clumped isotope temperature data to argue that the amplitude of late Miocene North Atlantic U$^{k'}_{37}$-SST cooling may have been overestimated due to seasonal bias in alkenone production.

Keeping in mind the potential biases in North Atlantic SST estimates and based on the assumption that SSTs from Site U1443 are representative of global low-latitude trends over the late Miocene, we estimate the evolution of proxy-derived meridional SST gradients and compare this to simulated meridional SST gradients. To calculate model-derived gradients, we averaged mean annual SSTs over the entire latitudinal band between 5 °S and 19 °N for the tropics and 48 °N and 70 °N for the northern high latitudes in the LM-560 and LM-300 simulations to represent condition at 8 ±0.5 Ma to 6 ±0.5 Ma, respectively. These latitudinal bands correspond to the regions covered by proxies-derived SST records used to estimate meridional gradients, taking into account their late Miocene paleolocations (Figure 7). To calculate proxy-derived meridional SST gradient evolution, we used the difference between tropical Mg/Ca-SST at Site U1443 and Northern Hemisphere high-latitude stacked $U^{k'}_{37}$-SST including the four sites in Herbert et al. (2016) (with revised age model at Site ODP 982 by Drury et al., 2018) (Figure 4c orange curve) and excluding North Atlantic ODP Site 982 where reconstructed $U^{k'}_{37}$-SSTs are particularly warm (mean value of 21.45 °C between 9 and 5 Ma) (Figure 4c red curve). From 8 ±0.5 Ma to 6 ±0.5 Ma, the data-based meridional gradient shows a 3.4 °C (2 °C) increase, depending on the inclusion (exclusion) of Site 982 in the northern high-latitude $U^{k'}_{37}$-SST stack. In comparison, when tropical stacked $U^{k'}_{37}$-SSTs are used in the calculation instead of U1443 Mg/Ca-SSTs, a much higher increase in meridional gradient of 4.7 °C (3.3 °C) is suggested, again dependant on the inclusion (exclusion) of Site 982 (Figure 5c dashed curves). On the other hand, simulated meridional SST gradients do not show a significant increase from 8 to 6 Ma and have a value of ~22 °C. This comparison reveals that estimations of meridional SST gradient evolution over the late Miocene using Site U1443 Mg/Ca-SST to represent the global low-latitude trend and stacked $U^{k'}_{37}$-SST (excluding North Atlantic Site 982) to represent the global Northern Hemisphere high-latitude trend result in a much better data-model agreement (Figure 4c). While meridional SST gradients calculated with U1443 Mg/Ca-derived SSTs as the tropical end-member are sensitive to scenarios for Mg/Ca$_{sw}$ evolution (Text S5), the increase in meridional SST gradient over time is systematically smaller than that reconstructed using tropical $U^{k'}_{37}$-SST estimates. These finding suggest that the choice of sites adapted to register global latitudinal trends and the choice of proxies adapted to reconstruct mean annual SST are crucial and could explain in part the discrepancies often observed between proxy- and model-derived SSTs and resultant estimates of meridional temperature gradients. These new results  suggest a much more

modest increase in meridional SSTs gradients during the LMGC than previously suggested by $U^{k'}_{37}$-SSTs stacks, with important implication regarding our comprehension of the late Miocene climate system (for example, estimations of polar amplification and the strength of atmospheric circulation and Hadley cells).

## 6 Conclusions

We present a new orbital-resolution equatorial Indian Ocean Mg/Ca-SST record spanning the interval from 9 to 5 Ma (late Miocene and earliest Pliocene) together with new late Miocene climate simulations under three plausible $p$CO$_2$ scenarios (300 ppm, 420 ppm and 560 ppm, in the range of $p$CO$_2$ proxy reconstructions). To date, this is the first late Miocene tropical SST record located in an open-ocean region with sufficient resolution to also resolve orbital scale variability. Our record shows a tropical SST cooling of 3.2 °C from 7.4 Ma until 5.8 Ma, similar in magnitude and timing to previously published mid-latitude $U^{k'}_{37}$-SST trends. Our data-model comparison supports the hypothesis that a near halving of $p$CO$_2$, from around 560 ppm before the LMGC to around 300 ppm at the end of the LMGC in our simulations, was required to drive global SST cooling, consistent with recent revised and new $p$CO$_2$ reconstructions (Brown et al., 2022 ; Mejia et al., 2017; Rae et al., 2021; Tanner et al., 2020) and with the $p$CO$_2$ decrease hypothesised in Herbert et al. (2016). $p$CO$_2$ forcing of SST can explain over two thirds of the cooling trend at Site U1443. In addition, time series analyses reveal a major increase in tropical (Sites U1443 and 1146) SST sensitivity to obliquity forcing at the onset of the LMGC, suggesting that tropical SSTs became more tightly coupled to glacial-interglacial climate during this time. Together, these results support the hypothesis that the late Miocene underwent a secular decrease in tropical SST mostly driven by atmospheric $p$CO$_2$ decrease, but with a much more modest increase in meridional SST gradients than previously suggested**.**

## Figure Captions

**Figure 1.** (a) Base map of inter-tropical modern mixed-layer depth (for June, data from ORAS5 Global Ocean Reanalysis - https://cds.climate.copernicus.eu/cdsapp#!/dataset/reanalysis-

), and sites with existing late Miocene SST reconstructions (symbols). Sites are placed at their average paleolocation between 8 and 6 Ma (paleolocations from PaleoAtlas for Gplates, Scotese, 2016). The amplitude of late Miocene SST cooling based on site-specific proxy records (colour within symbols) is calculated from averaged SSTs at 8 ±0.5 Ma minus 6 ±0.5 Ma. Squares indicate Mg/Ca-SST records, triangles indicate $TEX_{86}$-SST records and circles indicate $U^{k'}_{37}$-SST records. All SSTs were recalculated in a consistent way as described in the methods. The red square shows the paleolocation of Site U1443 studied here. (b) to (d): Modern oceanographic conditions at Site U1443 in the southern Bay of Bengal. Maps show seasonal SST and surface ocean circulation (arrows) during the summer (July, August, September) (b) and during the winter (January, February, March) (c). On both maps the modern location of IODP Site U1443 in the Bay of Bengal (black square) and its paleolocation at 9 Ma (latitude ~2.5°N and longitude ~89°E; black dot) are shown. Panel (d) shows modern monthly wind stress and mixed layer depth, with points representing individual months and diamonds with line representing monthly mean values over entire time series, and sea surface temperature and sea surface salinity with diamonds with lines corresponding to statistical mean of monthly mean values over entire time series with standard error bars, above Site U1443. Maps were created with Ocean Data View software using the SST datasets from the World Ocean Atlas 2013 (Locarnini et al., 2013). Paleolocation of Site U1443 was calculated from GPlates software using rotations and plate boundaries from the PALEOMAP PaleoAtlas for Gplates (Scotese, 2016). Ocean circulation is from Schott et al. (2009). SMC: Southwest Monsoon Current, NMC: Northeast Monsoon Current, SECC: South Equatorial Counter Current. In panel (c) wind stress is from ERDDAP (Wind Stress, Metop-A ASCAT, 0.25°, Global, Near Real Time, 2009-present), mixed layer depth (1969-2010) is from Keerthi et al. (2013), SST and SSS are from the World Ocean Atlas 2018 (Locarnini et al., 2018 and Zweng et al., 2018). Datasets were extracted for a box between 4.5-5.5°N latitude and 89-91°E longitude (depending on grid resolution) and binned by month. JJA: June, July, August, DJF: December, January, February.

**Figure 2.** Late Miocene to early Pliocene Mg/Ca-SST reconstruction from IODP Site U1443. (a) SST reconstruction derived from Mg/Ca ratios in *T. trilobus*, calculated using the Dekens et al. (2002) *T. sacculifer* equation for the Pacific Ocean. The blue curve shows SST uncorrected for Mg/Ca$_{sw}$ variation, and measured Mg/Ca ratios are also shown on the right axis. The red

curve is SST corrected for Mg/Ca$_{sw}$ variation following the scenario of HS15 (see section 3.2) with a linear relation between Mg/Ca$_{test}$ and Mg/Ca$_{sw}$ (H=1). The SST error envelopes correspond to ±1σ and ±2σ uncertainty (including analytical and age model errors) estimated using PSU Solver (Thirumalai et al., 2016). On the left axis the blue diamond represents mean core top Mg/Ca-SST with SD (blue error bar) and purple square represents mean annual SST for modern with max/min seasonal SST (purple error bar) (Holocene; 28.8 ±0.6 °C; G. Marino, unpublished and modern SST 28.8 °C +1.1 °C and -0.7 °C; World Ocean Atlas 2018). (b) Site U1443 benthic δ$^{18}$O (Bolton et al., 2022) with some Thvera-Gilbert (TG) cold stages indicated.

**Figure 3.** Time series analyses of Mg/Ca at Site U1443

All timeseries analyses were performed on resampled and bandpassed records as described in the methods (a) bandpassed Mg/Ca record (b) evolutive spectral analysis of Mg/Ca, (c) and (d) singular spectral analyses of Mg/Ca over two intervals: from 5 to 7.5 Ma, and from 7.5 to 9 Ma, respectively. (e) Cross-wavelet analyses of Site U1443 Mg/Ca and benthic δ$^{18}$O. Dashed line on evolutive, spectral and cross-wavelet analyses indicate periods of 404, 124, 95, 41, 24, 22 and 19 kyr resulting from Earth's orbital periods. Throughout, primary periods are shown in red and heterodynes in black.

**Figure 4**. Late Miocene global cooling, $p$CO$_2$ proxy data, and evolution of latitudinal thermal gradients. (a) Stacked SST anomalies based on U$^{K'}_{37}$ data for the tropics (grey curve), mid-latitudes (green and blue curves) and high northern latitudes (dark blue curve) from Herbert et al. (2016), with new U1443 Mg/Ca-SST (red curve). All data are shown as SST anomalies relative to the modern (left axis) and absolute SST values for Site U1443 are also shown (right axis). (b) Late Miocene $p$CO$_2$ proxy data compilation obtained from https://paleo-co2.org with data from Mejia et al., 2017, Tanner et al., 2020, Rae et al., 2021 and Brown et al., 2022 added. (c) Evolution of latitudinal SST gradients between Northern Hemisphere high latitudes and tropics. Red and orange curves are calculated using U1443 Mg/Ca-SST as representative of the tropical trend (although we acknowledge that this is a single-site record) minus the Northern Hemisphere high latitude U$^{K'}_{37}$-SST stack (Sites 883/884, 887, 907 and 982) (orange curve) and the U$^{K'}_{37}$-SST stack without North Atlantic Site 982 (red curve). Green and blue dashed curves are

calculated using the $U^{K'}_{37}$-SST tropical stack (Sites 722, 846, 850, 1241, U1338) minus Northern Hemisphere high latitudes $U^{K'}_{37}$-SST stack (blue dashed curve) and $U^{K'}_{37}$-SST stack without North Atlantic Site 982 (green dashed curve). Squares represent values of modelled latitudinal SST gradients at 8 ±0.5 Ma and 6 ±0.5 Ma corresponding to LM-560 and LM-300 simulations, respectively, using the mean annual SST average over the entire latitude band between 5°S and 19°N for the tropics and 48°N and 70°N for the high latitudes (see section 5.2.3). We note that absolute Mg/Ca-based SSTs reconstructed for Site U1443, and therefore ΔSST meridional values (red and orange curves), are sensitive to the choice of Mg/Ca$_{sw}$ correction (Fig. S4), yet all scenarios produce a smaller change in gradient over time.

**Figure 5.** Tropical high-resolution SST records for the late Miocene and earliest Pliocene (9 to 5 Ma).

(a) Mg/Ca-SST from equatorial Indian Ocean Site U1443, (b) Mg/Ca-SST from South China Sea Site 1146 (Holbourn et al., 2018) and (c) Mg/Ca-SST from Andaman Sea Site U1448 (Jöhnck et al., 2020). All SST records were recalculated using the same calibration and Mg/Ca$_{sw}$ correction as in Fig. 2., the thick curves are 10 % Lowess filters. (d) Site U1443 benthic (*C. wuellerstorfi*) $\delta^{13}$C (Bolton et al., 2022) and (e) Site U1443 benthic $\delta^{18}$O (Bolton et al., 2022) with Thvera-Gilbert (TG) cold stages marked. Blue shading represents the Late Miocene Global Cooling (LMGC) interval and grey shading represent the late Miocene carbon isotope shift (LMCIS). Horizontal blue and pink lines represent the intervals between which the amplitude of long-term SST changes (based on smoothed records) was calculated for the three sites. Intervals between pink and blue lines represent long-term cooling recorded at Sites U1443 and 1146 (LMGC). Intervals between blue and pink lines represent long-term warming recorded at Sites U1443, 1146 and U1448 (latest Miocene-early Pliocene warming).

**Figure 6.** Mean modelled latitudinal SST gradients and proxy-derived SSTs.
The LM-560 simulation (b) and LM-300 simulation (a) correspond to atmospheric CO$_2$ fixed at 560 ppm and 300 ppm, respectively, under late Miocene boundary conditions (see methods). In panel (b), LM-420 and LM-300 simulations are also shown with black and grey dashed lines, respectively. LM-560 and LM-300 simulations are compared to our global SST compilation from

proxies (Mg/Ca, $U^{K'}_{37}$ and $TEX_{86}$) in 1 Myr time windows centered on 8 Ma and 6 Ma, respectively. The grey envelope represents maximum and minimum mean annual SSTs at each latitude. All proxy-derived SSTs were recalculated in a consistent way (see Methods) and are plotted at their paleolatitude at 8 and 6 Ma (PaleoAtlas for Gplates, Scotese, 2016). In brief, Mg/Ca SSTs were recalculated as in Fig. 2 and 4, $U^{K'}_{37}$ SSTs were recalculated using the BAYSPLINE calibration (Tierney & Tingley, 2018), and $TEX_{86}$ SST were recalculated using the BAYSPAR Analog mode calibration (Tierney & Tingley, 2015).

**Figure 7.** Model-data comparison of the amplitude of the late Miocene cooling.

The map background color scale shows the SST anomaly from the LM-560 simulation minus the LM-300 simulation and indicates the amplitude of modelled late Miocene cooling that best fits with proxies-derived SSTs. Sites with available late Miocene SST records (symbols) are placed on the map at their average paleolocation between 8 and 6 Ma (paleolocation from PaleoAtlas for Gplates, Scotese, 2016). The amplitude of SST cooling based on site-specific proxy records (colour within symbols) is calculated from averaged SSTs at 8 ±0.5 Ma minus 6 ±0.5 Ma. Squares indicate Mg/Ca-SST records, triangles indicate $TEX_{86}$-SST records and circles indicate $U^{k'}_{37}$-SST records. All SSTs were recalculated in a consistent way as described in the caption of Figure 6. The same color scale is used for the map background and in the symbols.

France post-cruise funding (CTB), and a French Ministerial PhD scholarship awarded to C.M. C.M., C.T.B., K.T and A.C.S. designed the study. Sample processing was carried out by C.T.B and E.G. Picking and cleaning of planktic foraminifera was carried out by C.M and E.G. ICP-MS analyses were performed by M.G., and model simulations were performed by A.C.S. with Y.D. C.M. wrote the manuscript with contributions and feedback from C.T.B, K.T., A.C.S and Y.D.

## Open Research

All data generated for this study (Mg/Ca data, reconstructed SST and climatic simulations) are archived and publicly available via the PANGAEA data repository online (Martinot et al., 2022a and Martinot et al., 2022b). Core-top Mg/Ca data of Holocene age from ODP Site 758 provided by Gianluca Marino are presented in Table S1 in the Supporting Information.

## References

Allen, K. A., Hönisch, B., Eggins, S. M., Haynes, L. L., Rosenthal, Y., & Yu, J. (2016). Trace element proxies for surface ocean conditions: A synthesis of culture calibrations with planktic foraminifera. *Geochimica et Cosmochimica Acta*, *193*, 197-221. https://doi.org/10.1016/j.gca.2016.08.015

Anand, P., Elderfield, H., & Conte, M. H. (2003). Calibration of Mg/Ca thermometry in planktonic foraminifera from a sediment trap time series. *Paleoceanography*, *18*(2). https://doi.org/10.1029/2002PA000846

Andrae, J. W., McInerney, F. A., Polissar, P. J., Sniderman, J. M. K., Howard, S., Hall, P. A., & Phelps, S. R. (2018). Initial expansion of C4 vegetation in Australia during the late Pliocene. *Geophysical Research Letters*, *45*(10), 4831-4840. https://doi.org/10.1029/2018GL077833

Aumont, O., Éthé, C., Tagliabue, A., Bopp, L., & Gehlen, M. (2015). PISCES-v2: an ocean biogeochemical model for carbon and ecosystem studies. *Geoscientific Model Development*, *8*(8), 2465-2513. https://doi.org/10.5194/gmd-8-2465-2015

Badger, M. P., Chalk, T. B., Foster, G. L., Bown, P. R., Gibbs, S. J., Sexton, P. F., ... & Pancost, R. D. (2019). Insensitivity of alkenone carbon isotopes to atmospheric CO 2 at low to moderate CO 2 levels. *Climate of the Past*, *15*(2), 539-554.

Bailey, I., Foster, G. L., Wilson, P. A., Jovane, L., Storey, C. D., Trueman, C. N., & Becker, J. (2012). Flux and provenance of ice-rafted debris in the earliest Pleistocene sub-polar North Atlantic Ocean comparable to the last glacial maximum. *Earth and Planetary Science Letters*, *341*, 222-233. https://doi.org/10.1016/j.epsl.2012.05.034

Balco, G., & Rovey, C. W. (2010). Absolute chronology for major Pleistocene advances of the Laurentide Ice Sheet. *Geology*, *38*(9), 795-798. https://doi.org/10.1130/G30946.1

Barker, S., Greaves, M., & Elderfield, H. (2003). A study of cleaning procedures used for foraminiferal Mg/Ca paleothermometry. *Geochemistry, Geophysics, Geosystems*, *4*(9). https://doi.org/10.1029/2003GC000559

Bassinot, F. C., Beaufort, L., Vincent, E., Labeyrie, L. D., Rostek, F., Müller, P. J., ... & Lancelot, Y. (1994). Coarse fraction fluctuations in pelagic carbonate sediments from the tropical Indian Ocean: A 1500-kyr record of carbonate dissolution. *Paleoceanography*, *9*(4), 579-600. https://doi.org/10.1029/94PA00860

Bé, A.W.H. (1980). Gametogenic calcification in a spinose planktonic foraminifer, Globigerinoides sacculifer (Brady).*Marine Micropaleontology*, *5*, 283-310. https://doi.org/10.1016/0377-8398(80)90014-6

Bé, A.W.H., and Tolderlund, D.S., (1971). Distribution and ecology of living planktonic foraminifera in surface waters of the Atlantic and Indian Oceans: *in* Funnell, W. R., and Riedel, W. R. (eds.), The Micropaleontology of Oceans, Cambridge University Press, New York, p. 105-149.

Beerling, D. J., & Royer, D. L. (2011). Convergent cenozoic CO2 history. *Nature Geoscience*, *4*(7), 418-420. https://doi.org/10.1038/ngeo1186

Berner, R. A. (2004). A model for calcium, magnesium and sulfate in seawater over Phanerozoic time. *American Journal of Science*, *304*(5), 438-453. https://doi.org/10.2475/ajs.304.5.438

Betzler, C., Eberli, G. P., Kroon, D., Wright, J. D., Swart, P. K., Nath, B. N., ... & Young, J. R. (2016). The abrupt onset of the modern South Asian Monsoon winds. *Scientific reports*, *6*(1), 1-10. https://doi.org/10.1038/srep29838

Betzler, C., Eberli, G. P., Lüdmann, T., Reolid, J., Kroon, D., Reijmer, J. J. G., ... & Yao, Z. (2018). Refinement of Miocene sea level and monsoon events from the sedimentary archive of the Maldives (Indian Ocean). *Progress in Earth and Planetary Science*, *5*(1), 1-18. https://doi.org/10.1186/s40645-018-0165-x

Bialik, O. M., Auer, G., Ogawa, N. O., Kroon, D., Waldmann, N. D., & Ohkouchi, N. (2020). Monsoons, upwelling, and the deoxygenation of the northwestern Indian Ocean in response to middle to late Miocene global climatic shifts. *Paleoceanography and Paleoclimatology*, *35*(2). https://doi.org/ 10.1029/2019PA003762

Bolton, C. T., Gray, E., Kuhnt, W., Holbourn, A. E., Lübbers, J., Grant, K., ... & Andersen, N. (2022). Secular and orbital-scale variability of equatorial Indian Ocean summer monsoon winds during the late Miocene.
Climate of the Past, 18(4), 713-738.
https://dx.doi.org/10.5194/cp-18-713-2022

Bolton, C. T., Hernández-Sánchez, M. T., Fuertes, M. A., González-Lemos, S., Abrevaya, L., Mendez-Vicente, A., ... & Stoll, H. M. (2016). Decrease in coccolithophore calcification and CO2 since the middle Miocene. *Nature communications*, *7*(1), 1-13. https://doi.org/10.1038/ncomms10284

Bolton, C. T., & Stoll, H. M. (2013). Late Miocene threshold response of marine algae to carbon dioxide limitation. *Nature*, *500*(7464), 558-562. https://doi.org/10.1038/nature12448

Bosmans, J. H. C., Erb, M. P., Dolan, A. M., Drijfhout, S. S., Tuenter, E., Hilgen, F. J., ... & Lourens, L. J. (2018). Response of the Asian summer monsoons to idealized precession and obliquity forcing in a set of GCMs. *Quaternary Science Reviews*, *188*, 121-135. https://doi.org/10.1016/j.quascirev.2018.03.025

Boyle, E. A., & Keigwin, L. D. (1985). Comparison of Atlantic and Pacific paleochemical records for the last 215,000 years: Changes in deep ocean circulation and chemical inventories. *Earth and Planetary Science Letters*, *76*(1-2), 135-150. https://doi.org/10.1016/0012-821X(85)90154-2

Breecker, D. O., & Retallack, G. J. (2014). Refining the pedogenic carbonate atmospheric CO2 proxy and application to Miocene CO2. Palaeogeography, Palaeoclimatology, Palaeoecology, 406, 1-8.

Broecker, W. S., & Peng, T.-H. (1982). Tracers in the sea. Palisades, New York: Eldigo.

Brown, R. M., Chalk, T. B., Crocker, A. J., Wilson, P. A., & Foster, G. L. (2022). Late Miocene cooling coupled to carbon dioxide with Pleistocene-like climate sensitivity. *Nature Geoscience*, 1-7. https://doi.org/10.1038/s41561-022-00982-7

Brown, S. J., & Elderfield, H. (1996). Variations in Mg/Ca and Sr/Ca ratios of planktonic foraminifera caused by postdepositional dissolution: Evidence of shallow Mg-dependent dissolution. *Paleoceanography*, *11*(5), 543-551.

Burls, N. J., Bradshaw, C. D., De Boer, A. M., Herold, N., Huber, M., Pound, M., ... & Zhang, Z. (2021). Simulating Miocene warmth: insights from an opportunistic Multi-Model ensemble (MioMIP1). *Paleoceanography and Paleoclimatology*, e2020PA004054. https://doi.org/10.1029/2020PA004054

Cane, M. A., & Molnar, P. (2001). Closing of the Indonesian Seaway as the missing link between Pliocene East African aridi¢-cation and the Pacific. *Nature*, *6834*, 157-161. https://doi.org/10.1038/35075500

Carrapa, B., Clementz, M., & Feng, R. (2019). Ecological and hydroclimate responses to strengthening of the Hadley circulation in South America during the Late Miocene cooling. *Proceedings of the National Academy of Sciences*, *116*(20), 9747-9752. https://doi.org/10.1073/pnas.1810721116

Cerling, T. E. (1992). Use of carbon isotopes in paleosols as an indicator of the P (CO2) of the paleoatmosphere. Global Biogeochemical Cycles, 6(3), 307-314.

Cerling, T. E., Harris, J. M., MacFadden, B. J., Leakey, M. G., Quade, J., Eisenmann, V., & Ehleringer, J. R. (1997). Global vegetation change through the Miocene/Pliocene boundary. *Nature*, *389*(6647), 153-158. https://doi.org/10.1038/38229

Clemens, S. C., Kuhnt, W., LeVay, L. J., Anand, P., Ando, T., Bartol, M., ... & Hathorne, E. C. (2016). Site U1443. In *Proceedings of the International Ocean Discovery Program* (Vol. 353). doi:10.14379/iodp.proc.353.102.2016

Clement, A. C., Hall, A., & Broccoli, A. J. (2004). The importance of precessional signals in the tropical climate. *Climate Dynamics*, *22*(4), 327-341. https://doi.org/10.1007/s00382-003-0375-8

Coggon, R. M., Teagle, D. A., Smith-Duque, C. E., Alt, J. C., & Cooper, M. J. (2010). Reconstructing past seawater Mg/Ca and Sr/Ca from mid-ocean ridge flank calcium carbonate veins. *Science*, *327*(5969), 1114-1117. DOI: 10.1126/science.1182252

Conte, M. H., Sicre, M. A., Rühlemann, C., Weber, J. C., Schulte, S., Schulz-Bull, D., & Blanz, T. (2006). Global temperature calibration of the alkenone unsaturation index (UK′ 37) in surface waters and comparison with surface sediments. *Geochemistry, Geophysics, Geosystems*, *7*(2). https://doi.org/10.1029/2005GC001054

Conte, M. H., Thompson, A., Lesley, D., & Harris, R. P. (1998). Genetic and physiological influences on the alkenone/alkenoate versus growth temperature relationship in Emiliania huxleyi and Gephyrocapsa oceanica. *Geochimica et Cosmochimica Acta*, *62*(1), 51-68. https://doi.org/10.1016/S0016-7037(97)00327-X

Cotton, J. M., & Sheldon, N. D. (2012). New constraints on using paleosols to reconstruct atmospheric p CO2. Bulletin, 124(9-10), 1411-1423.

Dekens, P., D. Lea, D. Pak, and H. Spero (2002). Core top calibration of Mg/Ca in tropical foraminifera: Refining paleotemperature estimation, Geochem. Geophys. Geosyst., 3(4), 1022. https://doi.org/10.1029/2001GC000200

Delaney, M. L., Bé, A. W., & Boyle, E. A. (1985). Li, Sr, Mg, and Na in foraminiferal calcite shells from laboratory culture, sediment traps, and sediment cores. *Geochimica et Cosmochimica Acta*, *49*(6), 1327-1341. https://doi.org/10.1016/0016-7037(85)90284-4

Demicco, R. V., Lowenstein, T. K., Hardie, L. A., & Spencer, R. J. (2005). Model of seawater composition for the Phanerozoic. *Geology*, *33*(11), 877-880. https://doi.org/10.1130/G21945.1

De Nooijer, L. J., Van Dijk, I., Toyofuku, T., & Reichart, G. J. (2017). The impacts of seawater Mg/Ca and temperature on element incorporation in benthic foraminiferal calcite. *Geochemistry, Geophysics, Geosystems*, *18*(10), 3617-3630. https://doi.org/10.1002/2017GC007183

Dickens, G. R., & Backman, J. (2012). A comment on "Pliocene climate change of the Southwest Pacific and the impact of ocean gateways" by C. Karas, D. Nürnberg, R. Tiedemann, D. Garbe Schönberg, EPSL 301, 117–124 (2011). *Earth and Planetary Science Letters*, (331-332), 364-365. http://dx.doi.org/10.1016%2Fj.epsl.2011.07.030

Dickson, J. A. D. (2002). Fossil echinoderms as monitor of the Mg/Ca ratio of Phanerozoic oceans. *Science*, *298*(5596), 1222-1224. DOI: 10.1126/science.1075882

Dowsett, H. J., Foley, K. M., Stoll, D. K., Chandler, M. A., Sohl, L. E., Bentsen, M., ... & Zhang, Z. (2013). Sea surface temperature of the mid-Piacenzian ocean: a data-model comparison. *Scientific reports*, *3*(1), 1-8. https://doi.org/10.1038/srep02013

Drury, A. J., Lee, G. P., Gray, W. R., Lyle, M., Westerhold, T., Shevenell, A. E., & John, C. M. (2018). Deciphering the state of the late Miocene to early Pliocene equatorial Pacific. *Paleoceanography and Paleoclimatology*, *33*(3), 246-263. https://doi.org/10.1002/2017PA003245

Drury, A. J., Liebrand, D., Westerhold, T., Beddow, H. M., Hodell, D. A., Rohlfs, N., ... & Lourens, L. J. (2021). Climate, cryosphere and carbon cycle controls on Southeast Atlantic orbital-scale carbonate deposition since the Oligocene (30–0 Ma). *Climate of the Past*, *17*(5), 2091-2117. https://doi.org/10.5194/cp-17-2091-2021

Drury, A. J., Westerhold, T., Frederichs, T., Tian, J., Wilkens, R., Channell, J. E., ... & Röhl, U. (2017). Late Miocene climate and time scale reconciliation: Accurate orbital calibration from a deep-sea perspective. *Earth and Planetary Science Letters*, *475*, 254-266. https://doi.org/10.1016/j.epsl.2017.07.038

Drury, A. J., Westerhold, T., Hodell, D., & Röhl, U. (2018). Reinforcing the North Atlantic backbone: revision and extension of the composite splice at ODP Site 982. *Climate of the Past*, *14*(3), 321-338.

Dufresne, J.-L., Foujols, M.-A., Denvil, S., Caubel, A., Marti, O., Aumont, O., Balkanski, Y., Bekki, S., Bellenger, H., Benshila, R., Bony, S., Bopp, L., Braconnot, P., Brockmann, P., Cadule, P., Cheruy, F., Codron, F., Cozic, A., Cugnet, D., de Noblet, N., Duvel, J.-P., Ethé, C., Fairhead, L., Fichefet, T., Flavoni, S., Friedlingstein, P., Grandpeix, J.-Y., Guez, L., Guilyardi, E., Hauglustaine, D., Hourdin, F., Idelkadi, A., Ghattas, J., Joussaume, S., Kageyama, M., Krinner,

G., Labetoulle, S., Lahellec, A., Lefebvre, M.-P., Lefevre, F., Levy, C., Li, Z. X., Lloyd, J., Lott, F., Madec, G., Mancip, M., Marchand, M., Masson, S., Meurdesoif, Y., Mignot, J., Musat, I., Parouty, S., Polcher, J., Rio, C., Schulz, M., Swingedouw, D., Szopa, S., Talandier, C., Terray, P., Viovy, N., and Vuichard, N.(2013). Climate Change Projections Using the IPSL-CM5 Earth System Model: From CMIP3 to CMIP5, *Climate Dynamics*, 40, 2123-2165, https://doi.org/10.1007/s00382-012-1636-1, 2013.

Edgar, K. M., Anagnostou, E., Pearson, P. N., & Foster, G. L. (2015). Assessing the impact of diagenesis on δ11B, δ13C, δ18O, Sr/Ca and B/Ca values in fossil planktic foraminiferal calcite. *Geochimica et Cosmochimica Acta*, *166*, 189-209. https://doi.org/10.1016/j.gca.2015.06.018

Ekart, D. D., Cerling, T. E., Montanez, I. P., & Tabor, N. J. (1999). A 400 million year carbon isotope record of pedogenic carbonate: implications for paleoatmospheric carbon dioxide. American Journal of Science, 299(10), 805-827.

Elderfield, H., Vautravers, M., & Cooper, M. (2002). The relationship between shell size and Mg/Ca, Sr/Ca, δ$^{18}$O, and δ$^{13}$C of species of planktonic foraminifera. *Geochemistry, Geophysics, Geosystems*, *3*(8), 1-13. https://doi.org/10.1029/2001GC000194

Evans, D., Brierley, C., Raymo, M. E., Erez, J., & Müller, W. (2016). Planktic foraminifera shell chemistry response to seawater chemistry: Pliocene–Pleistocene seawater Mg/Ca, temperature and sea level change. *Earth and Planetary Science Letters*, *438*, 139-148. https://doi.org/10.1016/j.epsl.2016.01.013

Evans, D., & Müller, W. (2012). Deep time foraminifera Mg/Ca paleothermometry: Nonlinear correction for secular change in seawater Mg/Ca. *Paleoceanography*, *27*(4). https://doi.org/10.1029/2012PA002315

Fantle, M. S., & DePaolo, D. J. (2006). Sr isotopes and pore fluid chemistry in carbonate sediment of the Ontong Java Plateau: Calcite recrystallization rates and evidence for a rapid rise

in seawater Mg over the last 10 million years. *Geochimica et Cosmochimica Acta*, *70*(15), 3883-3904. https://doi.org/10.1016/j.gca.2006.06.009

Farkaš, J., Böhm, F., Wallmann, K., Blenkinsop, J., Eisenhauer, A., Van Geldern, R., ... & Veizer, J. (2007). Calcium isotope record of Phanerozoic oceans: Implications for chemical evolution of seawater and its causative mechanisms. *Geochimica et Cosmochimica Acta*, *71*(21), 5117-5134. https://doi.org/10.1016/j.gca.2007.09.004

Fedorov, A. V., Burls, N. J., Lawrence, K. T., & Peterson, L. C. (2015). Tightly linked zonal and meridional sea surface temperature gradients over the past five million years. *Nature Geoscience*, *8*(12), 975-980.

Fichefet, T., & Maqueda, M. M. (1997). Sensitivity of a global sea ice model to the treatment of ice thermodynamics and dynamics. *Journal of Geophysical Research: Oceans*, *102*(C6), 12609-12646. https://doi.org/10.1029/97JC00480

Franks, P. J., Royer, D. L., Beerling, D. J., Van de Water, P. K., Cantrill, D. J., Barbour, M. M., & Berry, J. A. (2014). New constraints on atmospheric $CO_2$ concentration for the Phanerozoic. *Geophysical Research Letters*, *41*(13), 4685-4694.

Friedrich, O., Schiebel, R., Wilson, P. A., Weldeab, S., Beer, C. J., Cooper, M. J., & Fiebig, J. (2012). Influence of test size, water depth, and ecology on Mg/Ca, Sr/Ca, $\delta^{18}O$ and $\delta^{13}C$ in nine modern species of planktic foraminifers. *Earth and Planetary Science Letters*, *319*, 133-145. https://doi.org/10.1016/j.epsl.2011.12.002

Gallagher, S. J., Wallace, M. W., Li, C. L., Kinna, B., Bye, J. T., Akimoto, K., & Torii, M. (2009). Neogene history of the West Pacific warm pool, Kuroshio and Leeuwin currents. *Paleoceanography*, *24*(1). https://doi.org/10.1029/2008PA001660

Goni, M. A., Hartz, D. M., Thunell, R. C., & Tappa, E. (2001). Oceanographic considerations for the application of the alkenone-based paleotemperature U37K′ index in the Gulf of

California. *Geochimica et Cosmochimica Acta*, *65*(4), 545-557. https://doi.org/10.1016/S0016-7037(00)00559-7

Gordon, A. L. (2005). Oceanography of the Indonesian seas and their throughflow. *Oceanography*, *18*(4), 14-27.

Gordon, A. L., & Fine, R. A. (1996). Pathways of water between the Pacific and Indian oceans in the Indonesian seas. *Nature*, *379*(6561), 146-149. https://doi.org/10.1038/379146a0

Gothmann, A. M., Stolarski, J., Adkins, J. F., Schoene, B., Dennis, K. J., Schrag, D. P., ... & Bender, M. L. (2015). Fossil corals as an archive of secular variations in seawater chemistry since the Mesozoic. *Geochimica et Cosmochimica Acta*, *160*, 188-208. https://doi.org/10.1016/j.gca.2015.03.018

Gouhier, T. C., Grinsted, A., and Simko, V. (2016). Package 'biwavelet' [code].

Gray, W. R., & Evans, D. (2019). Nonthermal influences on Mg/Ca in planktonic foraminifera: A review of culture studies and application to the last glacial maximum. *Paleoceanography and Paleoclimatology*, *34*(3), 306-315. https://doi.org/10.1029/2018PA003517

Greaves, M. J., Barker, S., Daunt, C., & Elderfield, H. (2005). Accuracy, standardisation and interlaboratory calibration standards for foraminiferal Mg/Ca thermometry [Technical Brief]. *G3 Geochemistry Geophysics Geosystems*, *6*(2). https://doi.org/10.1029/2004GC000790

Grimalt, J. O., Calvo, E., & Pelejero, C. (2001). Sea surface paleotemperature errors in UK′ 37 estimation due to alkenone measurements near the limit of detection. *Paleoceanography*, *16*(2), 226-232. https://doi.org/10.1029/1999PA000440

Grinsted, A., Moore, J. C., and Jevrejeva, S. (2004). Application of the cross wavelet transform and wavelet coherence to geophysical time series. https://doi.org/10.5194/npg-11-561-2004

Gupta, A. K., Yuvaraja, A., Prakasam, M., Clemens, S. C., & Velu, A. (2015). Evolution of the South Asian monsoon wind system since the late Middle Miocene. *Palaeogeography, Palaeoclimatology, Palaeoecology*, *438*, 160-167. https://doi.org/10.1016/j.palaeo.2015.08.006

Gupta, S. M., Fernandes, A. A., & Mohan, R. (1996). Tropical sea surface temperatures and the Earth's orbital eccentricity cycles. *Geophysical Research Letters*, *23*(22), 3159-3162. https://doi.org/10.1029/96GL02923

Hall, R. (2002). Cenozoic geological and plate tectonic evolution of SE Asia and the SW Pacific: computer-based reconstructions, model and animations. *Journal of Asian Earth Sciences*, *20*(4), 353-431. https://doi.org/10.1016/S1367-9120(01)00069-4

Hall, R. (2009). Southeast Asia's changing palaeogeography. *Blumea-Biodiversity, Evolution and Biogeography of Plants*, *54*(1-2), 148-161. https://doi.org/10.3767/000651909X475941

Hall, R., Audley-Charles, M. G., Banner, F. T., Hidayat, S., & Tobing, S. L. (1988). Late Palaeogene–Quaternary geology of Halmahera, Eastern Indonesia: initiation of a volcanic island arc. *Journal of the Geological Society*, *145*(4), 577-590. https://doi.org/10.1144/gsjgs.145.4.0577

Hall, R., Gower, D. J., Johnson, K. G., Richardson, J. E., Rosen, B. R., Rüber, L., & Williams, S. T. (2012). Sundaland and Wallacea: geology, plate tectonics and palaeogeography. *Biotic evolution and environmental change in Southeast Asia*, *32*, 78.

Haywood, A. M., Tindall, J. C., Dowsett, H. J., Dolan, A. M., Foley, K. M., Hunter, S. J., ... & Lunt, D. J. (2020). A return to large-scale features of Pliocene climate: the Pliocene Model Intercomparison Project Phase 2. *Climate of the Past*. https://doi.org/10.5194/cp-2019-145

Hemleben, C., Spindler, M., & Anderson, O. R. (2012). *Modern planktonic foraminifera*. Springer Science & Business Media.

Herbert, T. D., Lawrence, K. T., Tzanova, A., Peterson, L. C., Caballero-Gill, R., & Kelly, C. S. (2016). Late Miocene global cooling and the rise of modern ecosystems. *Nature Geoscience*, *9*(11), 843-847. https://doi.org/10.1038/ngeo2813

Herbert, T. D., Peterson, L. C., Lawrence, K. T., & Liu, Z. (2010). Tropical ocean temperatures over the past 3.5 million years. *science*, *328*(5985), 1530-1534. DOI: 10.1126/science.1185435

Higgins, J. A., & Schrag, D. P. (2012). Records of Neogene seawater chemistry and diagenesis in deep-sea carbonate sediments and pore fluids. *Earth and Planetary Science Letters*, *357*, 386-396. https://doi.org/10.1016/j.epsl.2012.08.030

Higgins, J. A., & Schrag, D. P. (2015). The Mg isotopic composition of Cenozoic seawater–evidence for a link between Mg-clays, seawater Mg/Ca, and climate. *Earth and Planetary Science Letters*, *416*, 73-81. https://doi.org/10.1016/j.epsl.2015.01.003

Hilgen, F., Zeeden, C., & Laskar, J. (2020). Paleoclimate records reveal elusive~ 200-kyr eccentricity cycle for the first time. *Global and Planetary Change*, *194*, 103296. https://doi.org/10.1016/j.gloplacha.2020.103296

Ho, S. L., & Laepple, T. (2015). Glacial cooling as inferred from marine temperature proxies TEXH86 and UK′ 37. *Earth and Planetary Science Letters*, *409*, 15-22. https://doi.org/10.1016/j.epsl.2014.10.033

Ho, S. L., & Laepple, T. (2016). Flat meridional temperature gradient in the early Eocene in the subsurface rather than surface ocean. *Nature Geoscience*, *9*(8), 606-610. https://doi.org/10.1038/ngeo2763

Hodell, D. A., Curtis, J. H., Sierro, F. J., & Raymo, M. E. (2001). Correlation of late Miocene to early Pliocene sequences between the Mediterranean and North Atlantic. *Paleoceanography*, *16*(2), 164-178. https://doi.org/10.1029/1999PA000487

Hodell, D. A., & Vayavananda, A. (1993). Middle Miocene paleoceanography of the western equatorial Pacific (DSDP site 289) and the evolution ofGloborotalia (Fohsella). *Marine Micropaleontology*, *22*(4), 279-310. https://doi.org/10.1016/0377-8398(93)90019-T

Holbourn, A., Kuhnt, W., Clemens, S. C., & Heslop, D. (2021). A~ 12 Myr Miocene Record of East Asian Monsoon variability from the South China Sea. *Paleoceanography and Paleoclimatology*, *36*(7), e2021PA004267.

Holbourn, A. E., Kuhnt, W., Clemens, S. C., Kochhann, K. G., Jöhnck, J., Lübbers, J., & Andersen, N. (2018). Late Miocene climate cooling and intensification of southeast Asian winter monsoon. *Nature Communications*, *9*(1), 1-13. https://doi.org/10.1038/s41467-018-03950-1

Holbourn, A., Kuhnt, W., Lyle, M., Schneider, L., Romero, O., & Andersen, N. (2014). Middle Miocene climate cooling linked to intensification of eastern equatorial Pacific upwelling. *Geology*, *42*(1), 19-22. https://doi.org/10.1130/G34890.1

Hollstein, M., Mohtadi, M., Rosenthal, Y., Moffa Sanchez, P., Oppo, D., Martínez Méndez, G., ... & Hebbeln, D. (2017). Stable oxygen isotopes and Mg/Ca in planktic foraminifera from modern surface sediments of the Western Pacific Warm Pool: Implications for thermocline reconstructions. *Paleoceanography*, *32*(11), 1174-1194. https://doi.org/10.1002/2017PA003122

Horita, J., H. Zimmermann, and H. Holland (2002). Chemical evolution of seawater during the Phanerozoic: Implications from the record of marine evaporites, Geochim. Cosmochim. Acta, 66(21), 3733–3756. https://doi.org/10.1016/S0016-7037(01)00884-5

Hourdin, F., Foujols, M. A., Codron, F., Guemas, V., Dufresne, J. L., Bony, S., ... & Bopp, L. (2013). Impact of the LMDZ atmospheric grid configuration on the climate and sensitivity of the IPSL-CM5A coupled model. *Climate Dynamics*, *40*(9-10), 2167-2192. DOI 10.1007/s00382-012-1411-3

Huang, Y., Clemens, S. C., Liu, W., Wang, Y., & Prell, W. L. (2007).Large-scale hydrological change drove the late Miocene C4 plant expansion in the Himalayan foreland and Arabian Peninsula. *Geology*, *35*(6), 531-534. https://doi.org/10.1130/G23666A.1

Jensen, T. G. (2001). Arabian Sea and Bay of Bengal exchange of salt and tracers in an ocean model. *Geophysical Research Letters*, *28*(20), 3967-3970. https://doi.org/10.1029/2001GL013422

Jensen, T. G. (2003). Cross-equatorial pathways of salt and tracers from the northern Indian Ocean: Modelling results. *Deep Sea Research Part II: Topical Studies in Oceanography*, *50*(12-13), 2111-2127. https://doi.org/10.1016/S0967-0645(03)00048-1

Ji, S., Nie, J., Lechler, A., Huntington, K. W., Heitmann, E. O., & Breecker, D. O. (2018). A symmetrical CO2 peak and asymmetrical climate change during the middle Miocene. *Earth and Planetary Science Letters*, *499*, 134-144.

Jöhnck, J., Kuhnt, W., Holbourn, A., & Andersen, N. (2020). Variability of the Indian Monsoon in the Andaman Sea Across the Miocene-Pliocene Transition. *Paleoceanography and Paleoclimatology*, *35*(9), e2020PA003923. https://doi.org/10.1029/2020PA003923

John, K. E. S., & Krissek, L. A. (2002). The late Miocene to Pleistocene ice-rafting history of southeast Greenland. *Boreas*, *31*(1), 28-35. https://doi.org/10.1111/j.1502-3885.2002.tb01053.x

Jonkers, L., Brummer, G. J. A., Peeters, F. J., van Aken, H. M., & De Jong, M. F. (2010). Seasonal stratification, shell flux, and oxygen isotope dynamics of left-coiling N. pachyderma and T. quinqueloba in the western subpolar North Atlantic. *Paleoceanography*, *25*(2). https://doi.org/10.1029/2009PA001849

Jonkers, L., Van Heuven, S., Zahn, R., & Peeters, F. J. (2013). Seasonal patterns of shell flux, δ18O and δ13C of small and large N. pachyderma (s) and G. bulloides in the subpolar North Atlantic. *Paleoceanography*, *28*(1), 164-174. https://doi.org/10.1002/palo.20018

Karas, C., Nürnberg, D., Tiedemann, R., & Garbe-Schönberg, D. (2011). Pliocene climate change of the Southwest Pacific and the impact of ocean gateways. *Earth and Planetary Science Letters*, *301*(1-2), 117-124.

Keerthi, M. G., Lengaigne, M., Vialard, J., de Boyer Montégut, C., & Muraleedharan, P. M. (2013). Interannual variability of the Tropical Indian Ocean mixed layer depth. *Climate dynamics*, *40*(3), 743-759. https://doi.org/10.1007/s00382-012-1295-2

Keigwin Jr, L. D. (1979). Late Cenozoic stable isotope stratigraphy and paleoceanography of DSDP sites from the east equatorial and central North Pacific Ocean. *Earth and Planetary Science Letters*, *45*(2), 361-382. https://doi.org/10.1016/0012-821X(79)90137-7

Keigwin, L. D., & Shackleton, N. J. (1980). Uppermost Miocene carbon isotope stratigraphy of a piston core in the equatorial Pacific. *Nature*, *284*(5757), 613-614. https://doi.org/10.1038/284613a0

Kennett, J.P., Keller, G., Srinivasan, M.S., (1985). Miocene planktonic foraminiferal biogeography and pale-oceanographic development of the Indo-Pacific region. *The Miocene Ocean: Paleoceanography and biogeography: Boulder, Colorado Geologic Society of America Memoir*, 197-236. https://doi.org/10.1130/MEM163-p197

Knorr, G., Butzin, M., Micheels, A., & Lohmann, G. (2011). A warm Miocene climate at low atmospheric CO2 levels. *Geophysical Research Letters*, *38*(20). https://doi.org/10.1029/2011GL048873

Kodama, K. P., & Hinnov, L. A. (2014). *Rock magnetic cyclostratigraphy* (Vol. 5). John Wiley & Sons. DOI:10.1002/9781118561294

Krebs, U., Park, W., & Schneider, B. (2011). Pliocene aridification of Australia caused by tectonically induced weakening of the Indonesian throughflow. *Palaeogeography,*

*Palaeoclimatology, Palaeoecology*, *309*(1-2), 111-117.
https://doi.org/10.1016/j.palaeo.2011.06.002

Krinner, G., Ciais, P., Viovy, N., & Friedlingstein, P. (2005). A simple parameterization of nitrogen limitation on primary productivity for global vegetation models. *Biogeosciences Discussions*, *2*(4), 1243-1282. https://doi.org/10.5194/bgd-2-1243-2005

Krissek, L. A. (1995). Late Cenozoic ice-rafting records from Leg 145 sites in the North Pacific: Late Miocene onset, late Pliocene intensification, and Plio-Pleistocene events. In *Proc. Ocean Drill. Program Sci. Results* (Vol. 145, pp. 179-194).

Kuhnt, W., Holbourn, A., Hall, R., Zuvela, M., & Käse, R. (2004). Neogene history of the Indonesian throughflow. *Continent-Ocean Interactions within East Asian Marginal Seas. Geophysical Monograph*, *149*, 299-320. https://doi.org/10.1029/149GM16

Kürschner, W. M., van der Burgh, J., Visscher, H., & Dilcher, D. L. (1996). Oak leaves as biosensors of late Neogene and early Pleistocene paleoatmospheric $CO_2$ concentrations. *Marine Micropaleontology*, *27*(1-4), 299-312. https://doi.org/10.1016/0377-8398(95)00067-4

LaRiviere, J. P., Ravelo, A. C., Crimmins, A., Dekens, P. S., Ford, H. L., Lyle, M., & Wara, M. W. (2012). Late Miocene decoupling of oceanic warmth and atmospheric carbon dioxide forcing. *Nature*, *486*(7401), 97-100. https://doi.org/10.1038/nature11200

Larsen, H. C., Saunders, A. D., Clift, P. D., Beget, J., Wei, W., & Spezzaferri, S. (1994). Seven million years of glaciation in Greenland. *Science*, *264*(5161), 952-955. DOI: 10.1126/science.264.5161.952

Lawrence, K. T., Herbert, T. D., Brown, C. M., Raymo, M. E., & Haywood, A. M. (2009). High- amplitude variations in North Atlantic sea surface temperature during the early Pliocene warm period. *Paleoceanography*, *24*(2).

Lawrence, K. T., Liu, Z., & Herbert, T. D. (2006). Evolution of the eastern tropical Pacific through Plio-Pleistocene glaciation. *Science*, *312*(5770), 79-83. https://doi.org/10.1126/science.1120395

Lawrence, K., Pearson, A., Castañeda, I., Ladlow, C., Peterson, L., & Lawrence, C. (2020). Comparison of Late Neogene UK′37 and TEX86 paleotemperature records from the Eastern Equatorial Pacific at orbital resolution. Paleoceanography and Paleoclimatology, 35(7), e2020PA003858.

Lea, D. W. (2004). The 100 000-yr cycle in tropical SST, greenhouse forcing, and climate sensitivity. *Journal of Climate*, *17*(11), 2170-2179. https://doi.org/10.1175/1520-0442(2004)017<2170:TYCITS>2.0.CO;2

Lea, D. W., Mashiotta, T. A., & Spero, H. J. (1999). Controls on magnesium and strontium uptake in planktonic foraminifera determined by live culturing. *Geochimica et Cosmochimica Acta*, *63*(16), 2369-2379. https://doi.org/10.1016/S0016-7037(99)00197-0

Lea, D. W., Pak, D. K., Belanger, C. L., Spero, H. J., Hall, M. A., & Shackleton, N. J. (2006). Paleoclimate history of Galapagos surface waters over the last 135,000 yr. *Quaternary Science Reviews*, *25*(11-12), 1152-1167. https://doi.org/10.1016/j.quascirev.2005.11.010

Lear, C. H., Elderfield, H., & Wilson, P. A. (2000). Cenozoic deep-sea temperatures and global ice volumes from Mg/Ca in benthic foraminiferal calcite. *science*, *287*(5451), 269-272. DOI: 10.1126/science.287.5451.269

Leduc, G., Garidel-Thoron, T. D., Kaiser, J., Bolton, C., & Contoux, C. (2017). Databases for sea surface paleotemperature based on geochemical proxies from marine sediments: implications for model-data comparisons. *Quaternaire. Revue de l'Association française pour l'étude du Quaternaire*, *28*(2), 201-216. https://doi.org/10.4000/quaternaire.8034

Levy, R. H., Meyers, S. R., Naish, T. R., Golledge, N. R., McKay, R. M., Crampton, J. S., ... & Kulhanek, D. K. (2019). Antarctic ice-sheet sensitivity to obliquity forcing enhanced through ocean connections. *Nature Geoscience*, *12*(2), 132-137. https://doi.org/10.1038/s41561-018-0284-4

Li, D., Zhao, M., & Tian, J. (2017). Low-high latitude interaction forcing on the evolution of the 400 kyr cycle in East Asian winter monsoon records during the last 2.8 Myr. *Quaternary Science Reviews*, *172*, 72-82. https://doi.org/10.1016/j.quascirev.2017.08.005

Li, L., Li, Q., Tian, J., Wang, P., Wang, H., & Liu, Z. (2011). A 4-Ma record of thermal evolution in the tropical western Pacific and its implications on climate change. *Earth and Planetary Science Letters*, *309*(1-2), 10-20. https://doi.org/10.1016/j.epsl.2011.04.016

Li, M., Hinnov, L., & Kump, L. (2019). Acycle: Time-series analysis software for paleoclimate research and education. *Computers & geosciences*, *127*, 12-22. https://doi.org/10.1016/j.cageo.2019.02.011

Li, Q., Li, B., Zhong, G., McGowran, B., Zhou, Z., Wang, J., & Wang, P. (2006). Late Miocene development of the western Pacific warm pool: Planktonic foraminifer and oxygen isotopic evidence. *Palaeogeography, Palaeoclimatology, Palaeoecology*, *237*(2-4), 465-482. https://doi.org/10.1016/j.palaeo.2005.12.019

Lipp, J. S., & Hinrichs, K. U. (2009). Structural diversity and fate of intact polar lipids in marine sediments. *Geochimica et Cosmochimica Acta*, *73*(22), 6816-6833. https://doi.org/10.1016/j.gca.2009.08.003

Liu, J., Tian, J., Liu, Z., Herbert, T. D., Fedorov, A. V., & Lyle, M. (2019). Eastern equatorial Pacific cold tongue evolution since the late Miocene linked to extratropical climate. *Science advances*, *5*(4), eaau6060. DOI: 10.1126/sciadv.aau6060

Liu, X., Huber, M., Foster, G. L., Leckie, R. M., & Zhang, Y. G. (2020, May). Persistent high latitude amplification over the past 10 million years. In *EGU General Assembly Conference Abstracts* (p. 597).

Liu, Z., Cleaveland, L. C., & Herbert, T. D. (2008). Early onset and origin of 100-kyr cycles in Pleistocene tropical SST records. *Earth and Planetary Science Letters*, *265*(3-4), 703-715. https://doi.org/10.1016/j.epsl.2007.11.016

Liu, Z., & Herbert, T. D. (2004). High-latitude influence on the eastern equatorial Pacific climate in the early Pleistocene epoch. *Nature*, *427*(6976), 720-723. https://doi.org/10.1038/nature02338

Locarnini, M., Mishonov, A. V., Baranova, O. K., Boyer, T. P., Zweng, M. M., Garcia, H. E., Reagan, J.R., Seidov, D., Weathers, K., Paver, C. R., and Smolyar, I. (2018). *World Ocean Atlas 2018, Volume 1: Temperature*. A. Mishonov Technical Ed.; NOAA Atlas NESDIS 81, 52pp. https://archimer.ifremer.fr/doc/00651/76338/

Locarnini, R., Mishonov, A. V., Antonov, J. I., Boyer, T. P., Garcia, H.E., Baranova, O.K., Zweng, M. M., Paver, C. R., Reagan, J. R., Johnson, D. R., Hamilton, M., and D. Seidov, D. (2013). *World Ocean Atlas 2013, Volume 1: Temperature.* S. Levitus, Ed., A. Mishonov Technical Ed.; NOAA Atlas NESDIS 73, 40 pp.

Lowenstein, T., M. Timofeeff, S. Brennan, L. Hardie, and R. Demicco (2001). Oscillations in Phanerozoic seawater chemistry: Evidence from fluid inclusions, Science, 294, 1086–1088. DOI: 10.1126/science.1064280

Lüthi, D., Le Floch, M., Bereiter, B., Blunier, T., Barnola, J. M., Siegenthaler, U., ... & Stocker, T. F. (2008). High-resolution carbon dioxide concentration record 650,000–800,000 years before present. *nature*, *453*(7193), 379-382. https://doi.org/10.1038/nature06949

Madec, G. (2016). NEMO ocean engine, Note du Pôle modélisation, Inst. Pierre-Simon Laplace, 406.

Madec, G. NEMO reference manual, ocean dynamics component: NEMO-OPA. *Preliminary version. Note du Pole de modélisation, Institut Pierre-Simon Laplace (IPSL), France*, 1288-1161 (2008).

Martinot, C., Bolton, C. T., Sarr, A. C., Donndieu, Y., Garcia, M., Gray, E., Tachikawa, K. (2022a): Mg/Ca ratios measured on planktic foraminifera species and reconstructed Sea Surface Temperature (SST) from IODP Site 353-U1443. [Dataset] *PANGAEA*, https://doi.org/10.1594/PANGAEA.941970

Martinot, C., Bolton, C. T., Sarr, A. C., Donndieu, Y., Garcia, M., Gray, E., Tachikawa, K. (2022b): Climatic simulation from the equatorial Indian Ocean. [Dataset] *PANGAEA*, https://doi.org/10.1594/PANGAEA.941973

Mashiotta, T. A., Lea, D. W., & Spero, H. J. (1999). Glacial–interglacial changes in Subantarctic sea surface temperature and δ18O-water using foraminiferal Mg. *Earth and Planetary Science Letters*, *170*(4), 417-432. https://doi.org/10.1016/S0012-821X(99)00116-8

Mathien-Blard, E., & Bassinot, F. (2009). Salinity bias on the foraminifera Mg/Ca thermometry: Correction procedure and implications for past ocean hydrographic reconstructions. *Geochemistry, Geophysics, Geosystems*, *10*(12). https://doi.org/10.1029/2008GC002353

Medina-Elizalde, M., Lea, D. W., & Fantle, M. S. (2008). Implications of seawater Mg/Ca variability for Plio-Pleistocene tropical climate reconstruction. *Earth and Planetary Science Letters*, *269*(3-4), 585-595. https://doi.org/10.1016/j.epsl.2010.08.016

Mejía, L. M., Bernasconi, S. M., Fernandez, A., Zhang, H., Guitian, J., Perez-Huerta, A., & Stoll, H. M. (2020, December). Coccolith clumped isotopes suggest a more modest Miocene North Atlantic polar amplification. In *AGU Fall Meeting Abstracts*(Vol. 2020, pp. PP001-0002).

Mejía, L. M., Méndez-Vicente, A., Abrevaya, L., Lawrence, K. T., Ladlow, C., Bolton, C., ... & Stoll, H. (2017). A diatom record of CO2 decline since the late Miocene. *Earth and Planetary Science Letters*, *479*, 18-33. https://doi.org/10.1016/j.epsl.2017.08.034

Micheels, A., Bruch, A. A., Uhl, D., Utescher, T., & Mosbrugger, V. (2007). A Late Miocene climate model simulation with ECHAM4/ML and its quantitative validation with terrestrial proxy data. Palaeogeography, Palaeoclimatology, Palaeoecology, 253(1-2), 251-270.

Miller, K. G., Browning, J. V., Schmelz, W. J., Kopp, R. E., Mountain, G. S., & Wright, J. D. (2020). Cenozoic sea-level and cryospheric evolution from deep-sea geochemical and continental margin records. *Science advances*, *6*(20), eaaz1346. DOI: 10.1126/sciadv.aaz1346

Mix, A. C. (2003). Chapter 12, Site 1241. In *Proc. Ocean Drill. Program Initial Rep* (Vol. 202, p. 101). DOI:10.2973/odp.proc.ir.202.112.2003

Molnar, P., & Cronin, T. W. (2015). Growth of the Maritime Continent and its possible contribution to recurring Ice Ages. *Paleoceanography*, *30*(3), 196-225. https://doi.org/10.1002/2014PA002752

Mudelsee, M., & Raymo, M. E. (2005). Slow dynamics of the Northern Hemisphere glaciation. *Paleoceanography*, *20*(4). https://doi.org/10.1029/2005PA001153

Müller, P. J., Kirst, G., Ruhland, G., Von Storch, I., & Rosell-Melé, A. (1998). Calibration of the alkenone paleotemperature index U37K′ based on core-tops from the eastern South Atlantic and the global ocean (60° N-60° S). *Geochimica et Cosmochimica Acta*, *62*(10), 1757-1772. https://doi.org/10.1016/S0016-7037(98)00097-0

Nathan, S. A., & Leckie, R. M. (2009). Early history of the Western Pacific Warm Pool during the middle to late Miocene (~ 13.2–5.8 Ma): Role of sea-level change and implications for equatorial circulation. *Palaeogeography, Palaeoclimatology, Palaeoecology*, *274*(3-4), 140-159. https://doi.org/10.1016/j.palaeo.2009.01.007

O'Brien, C. L., Foster, G. L., Martínez-Botí, M. A., Abell, R., Rae, J. W., & Pancost, R. D. (2014). High sea surface temperatures in tropical warm pools during the Pliocene. *Nature Geoscience*, *7*(8), 606-611. https://doi.org/10.1038/ngeo2194

Ohneiser, C., Florindo, F., Stocchi, P., Roberts, A. P., DeConto, R. M., & Pollard, D. (2015). Antarctic glacio-eustatic contributions to late Miocene Mediterranean desiccation and reflooding. *Nature communications*, *6*(1), 1-10. https://doi.org/10.1038/ncomms9765

Otto-Bliesner, B. L., Jahn, A., Feng, R., Brady, E. C., Hu, A., & Löfverström, M. (2017). Amplified North Atlantic warming in the late Pliocene by changes in Arctic gateways. *Geophysical Research Letters*, *44*(2), 957-964. https://doi.org/10.1002/2016GL071805

Pagani, M., Freeman, K. H., & Arthur, M. A. (1999). Late Miocene atmospheric CO2 concentrations and the expansion of C4 grasses. *Science*, *285*(5429), 876-879. DOI: 10.1126/science.285.5429.876

Pagani, M., Liu, Z., LaRiviere, J., & Ravelo, A. C. (2010). High Earth-system climate sensitivity determined from Pliocene carbon dioxide concentrations. *Nature Geoscience*, *3*(1), 27-30.

Pagani, M., Zachos, J. C., Freeman, K. H., Tipple, B., & Bohaty, S. (2005). Marked decline in atmospheric carbon dioxide concentrations during the Paleogene. *Science*, *309*(5734), 600-603. DOI: 10.1126/science.1110063

Past Interglacials Working Group of PAGES. (2016). Interglacials of the last 800,000 years. *Reviews of Geophysics*, *54*(1), 162-219.

Pearson, P. N., & Palmer, M. R. (2000). Atmospheric carbon dioxide concentrations over the past 60 million years. *Nature*, *406*(6797), 695-699.

Pelejero, C., & Calvo, E. (2003). The upper end of the UK′ 37 temperature calibration revisited. *Geochemistry, Geophysics, Geosystems*, *4*(2). https://doi.org/10.1029/2002GC000431

Petit, J. R., Jouzel, J., Raynaud, D., Barkov, N. I., Barnola, J. M., Basile, I., ... & Stievenard, M. (1999). Climate and atmospheric history of the past 420,000 years from the Vostok ice core, Antarctica. *Nature*, *399*(6735), 429-436. https://doi.org/10.1038/20859

Poole, C. R., & Wade, B. S. (2019). Systematic taxonomy of the Trilobatus sacculifer plexus and descendant Globigerinoidesella fistulosa (planktonic foraminifera). *Journal of Systematic Palaeontology*, *17*(23), 1989-2030. https://doi.org/10.1080/14772019.2019.1578831

Pound, M. J., Haywood, A. M., Salzmann, U., & Riding, J. B. (2012). Global vegetation dynamics and latitudinal temperature gradients during the Mid to Late Miocene (15.97–5.33 Ma). *Earth-Science Reviews*, *112*(1-2), 1-22. https://doi.org/10.1016/j.earscirev.2012.02.005

Prahl, F. G., Muehlhausen, L. A., & Zahnle, D. L. (1988). Further evaluation of long-chain alkenones as indicators of paleoceanographic conditions. *Geochimica et Cosmochimica Acta*, *52*(9), 2303-2310. https://doi.org/10.1016/0016-7037(88)90132-9

Rae, J. W., Zhang, Y. G., Liu, X., Foster, G. L., Stoll, H. M., & Whiteford, R. D. (2021). Atmospheric CO2 over the Past 66 Million Years from Marine Archives. *Annual Review of Earth and Planetary Sciences*, *49*. https://doi.org/10.1146/annurev-earth-082420-063026

Ramaswamy, V., & Gaye, B. (2006). Regional variations in the fluxes of foraminifera carbonate, coccolithophorid carbonate and biogenic opal in the northern Indian Ocean. *Deep Sea Research Part I: Oceanographic Research Papers*, *53*(2), 271-293. https://doi.org/10.1016/j.dsr.2005.11.003

Rao, R. R., & Sivakumar, R. (2003). Seasonal variability of sea surface salinity and salt budget of the mixed layer of the north Indian Ocean. *Journal of Geophysical Research: Oceans*, *108*(C1), 9-1. https://doi.org/10.1029/2001JC000907

Retallack, G. J. (2009). Greenhouse crises of the past 300 million years. *Geological Society of America Bulletin*, *121*(9-10), 1441-1455. https://doi.org/10.1130/B26341.1

Reuss, A. V. (1850). Neues Foraminiferen aus den schicten des Osterreichischen Tertiarbeckens. *Denkschriften der Akademie des Wissenschaften Wein*, *1*, 365-390.

Richey, J. N., & Tierney, J. E. (2016). GDGT and alkenone flux in the northern Gulf of Mexico: Implications for the TEX86 and UK'37 paleothermometers. *Paleoceanography*, *31*(12), 1547-1561. https://doi.org/10.1002/2016PA003032

Rixen, T., Gaye, B., Emeis, K. C., & Ramaswamy, V. (2019). The ballast effect of lithogenic matter and its influences on the carbon fluxes in the Indian Ocean. *Biogeosciences*, *16*(2), 485-503. https://doi.org/10.5194/bg-16-485-2019

Rommerskirchen, F., Condon, T., Mollenhauer, G., Dupont, L., & Schefuss, E. (2011). Miocene to Pliocene development of surface and subsurface temperatures in the Benguela Current system. *Paleoceanography*, *26*(3).  https://doi.org/10.1029/2010PA002074

Rosenthal, Y., & Lohmann, G. P. (2002). Accurate estimation of sea surface temperatures using dissolution-corrected calibrations for Mg/Ca paleothermometry. *Paleoceanography*, *17*(3), 16-1. https://doi.org/10.1029/2001PA000749

Rosenthal, Y., Lohmann, G. P., Lohmann, K. C., & Sherrell, R. M. (2000). Incorporation and preservation of Mg in Globigerinoides sacculifer: Implications for reconstructing the temperature and 18O/16O of seawater. *Paleoceanography*, *15*(1), 135-145. https://doi.org/10.1029/1999PA000415

Rosenthal, Y., Perron-Cashman, S., Lear, C. H., Bard, E., Barker, S., Billups, K., ... & Elderfield, H. (2004). Interlaboratory comparison study of Mg/Ca and Sr/Ca measurements in planktonic

foraminifera for paleoceanographic research. *Geochemistry, Geophysics, Geosystems*, *5*(4). https://doi.org/10.1029/2003GC000650

Rousselle, G., Beltran, C., Sicre, M. A., Raffi, I., & De Rafelis, M. (2013). Changes in sea-surface conditions in the Equatorial Pacific during the middle Miocene–Pliocene as inferred from coccolith geochemistry. *Earth and planetary science letters*, *361*, 412-421. https://doi.org/10.1016/j.epsl.2012.11.003

Sarr, A.-C., Donnadieu, Y. Bolton, C.T., Ladant, J.-B., Licht, A., Fluteau, F., Laugié, M. Tardif, D. and Dupont-Nivet, G.. (2022). Neogene South Asian monsoon rainfall and wind histories diverged due to topographic effects. *Nature Geoscience* 15, no. 4 (2022): 314-319.

Schiebel, R., & Hemleben, C. (2017). *Planktic foraminifers in the modern ocean* (pp. 1-358). Berlin: Springer. DOI 10.1007/978-3-662-50297-6

Schott, F. A., Xie, S. P., & McCreary Jr, J. P. (2009). Indian Ocean circulation and climate variability. *Reviews of Geophysics*, *47*(1). https://doi.org/10.1029/2007RG000245

Scotese, C. R. (2016). Tutorial: PALEOMAP PaleoAtlas for GPlates and the PaleoData Plotter Program. http://www.earthbyte.org/paleomap-paleoatlas-for-gplates/

Seki, O., Schmidt, D. N., Schouten, S., Hopmans, E. C., Sinninghe Damsté, J. S., & Pancost, R. D. (2012). Paleoceanographic changes in the Eastern Equatorial Pacific over the last 10 Myr. *Paleoceanography*, *27*(3). https://doi.org/10.1029/2011PA002158

Sepulchre, P., Caubel, A., Ladant, J. B., Bopp, L., Boucher, O., Braconnot, P., ... & Tardif, D. (2020). IPSL-CM5A2–an Earth system model designed for multi-millennial climate simulations. *Geoscientific Model Development*, *13*(7), 3011-3053. https://doi.org/10.5194/gmd-13-3011-2020

Sexton, P. F., Wilson, P. A., & Pearson, P. N. (2006). Microstructural and geochemical perspectives on planktic foraminiferal preservation:"Glassy" versus "Frosty". *Geochemistry, Geophysics, Geosystems*, *7*(12). https://doi.org/10.1029/2006GC001291

Shackleton, N. J., Hall, M. A., & Pate, D. (1995). 15. Pliocene stable isotope stratigraphy of Site 846. In *Proc. Ocean Drill. Program Sci. Results* (Vol. 138, pp. 337-355).

Shetye, S. R., Gouveia, A. D., Shankar, D., Shenoi, S. S. C., Vinayachandran, P. N., Sundar, D., ... & Nampoothiri, G. (1996). Hydrography and circulation in the western Bay of Bengal during the northeast monsoon. *Journal of Geophysical Research: Oceans*, *101*(C6), 14011-14025. https://doi.org/10.1029/95JC03307

Shipboard Scientific Party, (1989). Site 758. *In* Peirce, J., Weissel, J., et al., *Proc. ODP, Init. Repts.,* 121: College Station, TX (Ocean Drilling Program), 359–453.

Sonzogni, C., Bard, E., & Rostek, F. (1998). Tropical sea-surface temperatures during the last glacial period: A view based on alkenones in Indian Ocean sediments. *Quaternary Science Reviews*, *17*(12), 1185–1201. https://doi.org/10.1016/S0277-3791(97)00099-1

Sosdian, S. M., Greenop, R., Hain, M. P., Foster, G. L., Pearson, P. N., & Lear, C. H. (2018). Constraining the evolution of Neogene ocean carbonate chemistry using the boron isotope pH proxy. *Earth and Planetary Science Letters*, *498*, 362-376. https://doi.org/10.1016/j.epsl.2018.06.017

Sosdian, S. M., & Lear, C. H. (2020). Initiation of the Western Pacific Warm Pool at the Middle Miocene Climate Transition?. *Paleoceanography and Paleoclimatology*, *35*(12), e2020PA003920. https://doi.org/10.1029/2020PA003920

Spahni, R., Chappellaz, J., Stocker, T. F., Loulergue, L., Hausammann, G., Kawamura, K., ... & Jouzel, J. (2005). Atmospheric methane and nitrous oxide of the late Pleistocene from Antarctic ice cores. *Science*, *310*(5752), 1317-1321. DOI: 10.1126/science.abd2897

Spezzaferri, S. (1994). Planktonic foraminiferal biostratigraphy and taxonomy of the Oligocene and lower Miocene in the oceanic record. An overview. Pacini Editore.

Spezzaferri, S., Kucera, M., Pearson, P. N., Wade, B. S., Rappo, S., Poole, C. R., ... & Stalder, C. (2015). Fossil and Genetic Evidence for the Polyphyletic Nature of the Planktonic Foraminifera" Globigerinoides", and Description of the New Genus Trilobatus. *PLoS One*, *10*(5), e0128108. https://doi.org/10.1371/journal.pone.0128108

Stanley, S. M., & Hardie, L. A. (1998). Secular oscillations in the carbonate mineralogy of reef-building and sediment-producing organisms driven by tectonically forced shifts in seawater chemistry. *Palaeogeography, Palaeoclimatology, Palaeoecology*, *144*(1-2), 3-19. https://doi.org/10.1016/S0031-0182(98)00109-6

Stap, L,B,, de Boer, B,, Ziegler, M,, Bintanja, R,, Lourens, L,J, and van de Wal, R,S,W, (2016) CO2 over the past 5 million years: Continuous simulation and new δ11B-based proxy data, Earth and Planetary Science Letters 439, 1-26

Steinke, S., Groeneveld, J., Johnstone, H., & Rendle-Bühring, R. (2010). East Asian summer monsoon weakening after 7.5 Ma: evidence from combined planktonic foraminifera Mg/Ca and δ18O (ODP Site 1146; northern South China Sea). *Palaeogeography, Palaeoclimatology, Palaeoecology*, *289*(1-4), 33-43. https://doi.org/10.1016/j.palaeo.2010.02.007

Steinthorsdottir, M., Coxall, H. K., De Boer, A. M., Huber, M., Barbolini, N., Bradshaw, C. D., ... & Strömberg, C. A. E. (2021). The Miocene: The future of the past. *Paleoceanography and Paleoclimatology*, *36*(4), e2020PA004037. https://doi.org/10.1029/2020PA004037

Stoll, H. M., Guitian, J., Hernandez-Almeida, I., Mejia, L. M., Phelps, S., Polissar, P., ... & Ziveri, P. (2019). Upregulation of phytoplankton carbon concentrating mechanisms during low CO2 glacial periods and implications for the phytoplankton pCO2 proxy. *Quaternary Science Reviews*, *208*, 1-20. https://doi.org/10.1016/j.quascirev.2019.01.012

Stoll, H. M., Schrag, D. P., & Clemens, S. C. (1999). Are seawater Sr/Ca variations preserved in Quaternary foraminifera?. *Geochimica et Cosmochimica Acta*, *63*(21), 3535-3547. https://doi.org/10.1016/S0016-7037(99)00129-5

Stults, D. Z., Wagner-Cremer, F., & Axsmith, B. J. (2011). Atmospheric paleo-CO2 estimates based on Taxodium distichum (Cupressaceae) fossils from the Miocene and Pliocene of Eastern North America. *Palaeogeography, Palaeoclimatology, Palaeoecology*, *309*(3-4), 327-332. https://doi.org/10.1016/j.palaeo.2011.06.017

Super, J. R., Thomas, E., Pagani, M., Huber, M., O'Brien, C. L., & Hull, P. M. (2020). Miocene Evolution of North Atlantic Sea Surface Temperature. *Paleoceanography and Paleoclimatology*, *35*(5), e2019PA003748. https://doi.org/10.1029/2019PA003748

Tanner, T., Hernández-Almeida, I., Drury, A. J., Guitián, J., & Stoll, H. (2020). Decreasing atmospheric CO2 during the late Miocene Cooling. *Paleoceanography and Paleoclimatology*, e2020PA003925. https://doi.org/10.1029/2020PA003925

Tauxe, L., & Feakins, S. J. (2020). A reassessment of the chronostratigraphy of late Miocene C3–C4 transitions. *Paleoceanography and Paleoclimatology*, *35*(7), e2020PA003857. https://doi.org/10.1029/2020PA003857

Thadathil, P., Muraleedharan, P. M., Rao, R. R., Somayajulu, Y. K., Reddy, G. V., & Revichandran, C. (2007). Observed seasonal variability of barrier layer in the Bay of Bengal. *Journal of Geophysical Research: Oceans*, *112*(C2). https://doi.org/10.1029/2006JC003651

Thirumalai, K., Quinn, T. M. & Marino, G. (2016). Constraining past seawater $\delta^{18}O$ and temperature records developed from foraminiferal geochemistry. Paleoceanography 31, 1409-1422. https://doi.org/10.1002/2016PA002970

Thomas, E. K., Clemens, S. C., Sun, Y., Prell, W. L., Huang, Y., Gao, L., ... & Liu, Z. (2016). Heterodynes dominate precipitation isotopes in the East Asian monsoon region, reflecting interaction of multiple climate factors. *Earth and Planetary Science Letters*, *455*, 196-206. https://doi.org/10.1016/j.epsl.2016.09.044

Thomson, D.J., 1982. Spectrum estimation and harmonic analysis. Proceedings of the IEEE 70, 1055- 1096. https://doi.org/10.1109/PROC.1982.12434

Tian, J., Ma, W., Lyle, M. W., & Shackford, J. K. (2014). Synchronous mid-Miocene upper and deep oceanic δ13C changes in the east equatorial Pacific linked to ocean cooling and ice sheet expansion. *Earth and Planetary Science Letters*, *406*, 72-80. https://doi.org/10.1016/j.epsl.2014.09.013

Tierney, J. E., Malevich, S. B., Gray, W., Vetter, L., & Thirumalai, K. (2019). Bayesian calibration of the Mg/Ca paleothermometer in planktic foraminifera. *Paleoceanography and Paleoclimatology*, *34*(12), 2005-2030. https://doi.org/10.1029/2019PA003744

Tierney, J. E., & Tingley, M. P. (2015). A TEX 86 surface sediment database and extended Bayesian calibration. *Scientific data*, *2*(1), 1-10. https://doi.org/10.1038/sdata.2015.29

Tierney, J. E., & Tingley, M. P. (2018). BAYSPLINE: A new calibration for the alkenone paleothermometer. *Paleoceanography and Paleoclimatology*, *33*(3), 281-301. https://doi.org/10.1002/2017PA003201

Timmermann, R., Goosse, H., Madec, G., Fichefet, T., Ethe, C., & Duliere, V. (2005). On the representation of high latitude processes in the ORCA-LIM global coupled sea ice–ocean model. *Ocean Modelling*, *8*(1-2), 175-201. https://doi.org/10.1016/j.ocemod.2003.12.009

Tomczak M, Godfrey JS (2001) Regional Oceanography: an introduction, Chapter 11, The Indian Ocean, pp 175–198, Chapter 12, hydrology of the Indian Ocean pp199-214.

Tripati, A. K., Roberts, C. D., & Eagle, R. A. (2009). Coupling of CO2 and ice sheet stability over major climate transitions of the last 20 million years. *science*, *326*(5958), 1394-1397.

Unger, D., Ittekkot, V., Schäfer, P., Tiemann, J., & Reschke, S. (2003). Seasonality and interannual variability of particle fluxes to the deep Bay of Bengal: influence of riverine input and oceanographic processes. *Deep Sea Research Part II: Topical Studies in Oceanography*, *50*(5), 897-923. https://doi.org/10.1016/S0967-0645(02)00612-4

Valcke, S. (2013). The OASIS3 coupler: A European climate modelling community software. *Geoscientific Model Development*, *6*(2), 373-388. https://doi.org/10.5194/gmd-6-373-2013

Van der Weijst, C. M., van der Laan, K. J., Peterse, F., Reichart, G. J., Sangiorgi, F., Schouten, S., ... & Sluijs, A. (2021). A fifteen-million-year surface-and subsurface-integrated TEX 86 temperature record from the eastern equatorial Atlantic. *Climate of the Past Discussions*, 1-23. https://doi.org/10.5194/cp-2021-92

Vidya, P. J., Prasanna Kumar, S., Gauns, M., Verenkar, A., Unger, D., & Ramaswamy, V. (2013). Influence of physical and biological processes on the seasonal cycle of biogenic flux in the equatorial Indian Ocean. *Biogeosciences*, *10*(11), 7493-7507. https://doi.org/10.5194/bg-10-7493-2013

Vinayachandran, P. N., & Shetye, S. R. (1991). The warm pool in the Indian Ocean. *Proceedings of the Indian Academy of Sciences-Earth and Planetary Sciences*, *100*(2), 165-175. https://doi.org/10.1007/BF02839431

Visser, K., Thunell, R., & Stott, L. (2003). Magnitude and timing of temperature change in the Indo-Pacific warm pool during deglaciation. *Nature*, *421*(6919), 152-155. https://doi.org/10.1038/nature01297

Warnke, D. A., Allen, C. P., Muller, D. W., Hodell, D. A., & Brunner, C. A. (1992). Miocene-Pliocene Antarctic glacial evolution: A synthesis of ice-rafted debris, stable isotope, and planktonic foraminiferal indicators, ODP Leg 114. *The Antarctic Paleoenvironment: A Perspective on Global Change: Part One*, *56*, 311-326. https://doi.org/10.1029/AR056p0311

Webster, P. J., Magana, V. O., Palmer, T. N., Shukla, J., Tomas, R. A., Yanai, M. U., & Yasunari, T. (1998). Monsoons: Processes, predictability, and the prospects for prediction. *Journal of Geophysical Research: Oceans*, *103*(C7), 14451-14510. https://doi.org/10.1029/97JC02719

Westerhold, T., Marwan, N., Drury, A. J., Liebrand, D., Agnini, C., Anagnostou, E., ... & Zachos, J. C. (2020). An astronomically dated record of Earth's climate and its predictability over the last 66 million years. *Science*, *369*(6509), 1383-1387. DOI: 10.1126/science.aba6853

Wilkinson, B. H. & Algeo, T. J. (1989). Sedimentary carbonate record of calcium-magnesium cycling. *American Journal of Science*, *289*, 1158-1194. https://doi.org/10.2475/ajs.289.10.1158

Yan, X. H., Ho, C. R., Zheng, Q., & Klemas, V. (1992). Temperature and size variabilities of the Western Pacific Warm Pool. *Science*, *258*(5088), 1643-1645. DOI: 10.1126/science.258.5088.1643

You, Y., & Tomczak, M. (1993). Thermocline circulation and ventilation in the Indian Ocean derived from water mass analysis. *Deep Sea Research Part I: Oceanographic Research Papers*, *40*(1), 13-56. https://doi.org/10.1016/0967-0637(93)90052-5

Zhang, Y. G., Pagani, M., & Liu, Z. (2014). A 12-million-year temperature history of the tropical Pacific Ocean. *Science*, *344*(6179), 84- 87. DOI: 10.1126/science.1246172

Zhang, Y. G., Pagani, M., Liu, Z., Bohaty, S. M., & DeConto, R. (2013). A 40-million-year history of atmospheric CO2. *Philosophical Transactions of the Royal Society A: Mathematical,*

*Physical and Engineering Sciences*, *371*(2001), 20130096.
https://doi.org/10.1098/rsta.2013.0096

Zhang, Z., Ramstein, G., Schuster, M., Li, C., Contoux, C., & Yan, Q. (2014). Aridification of the Sahara desert caused by Tethys Sea shrinkage during the Late Miocene. *Nature*, *513*(7518), 401-404. https://doi.org/10.1038/nature13705
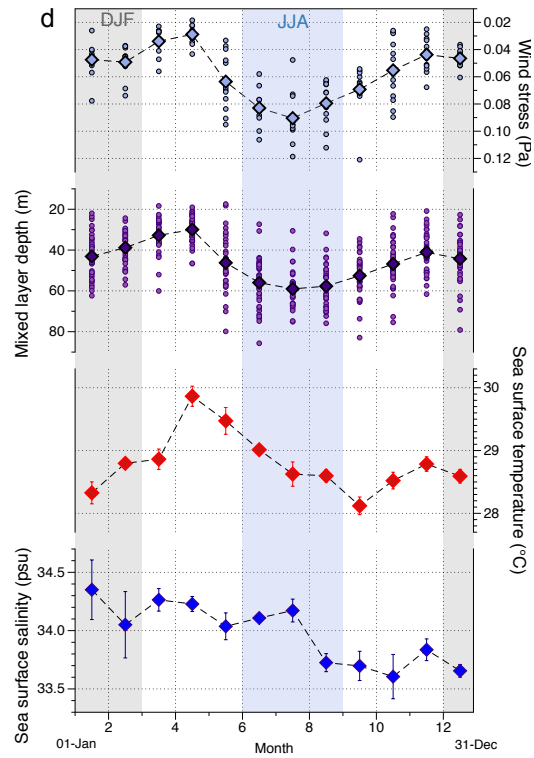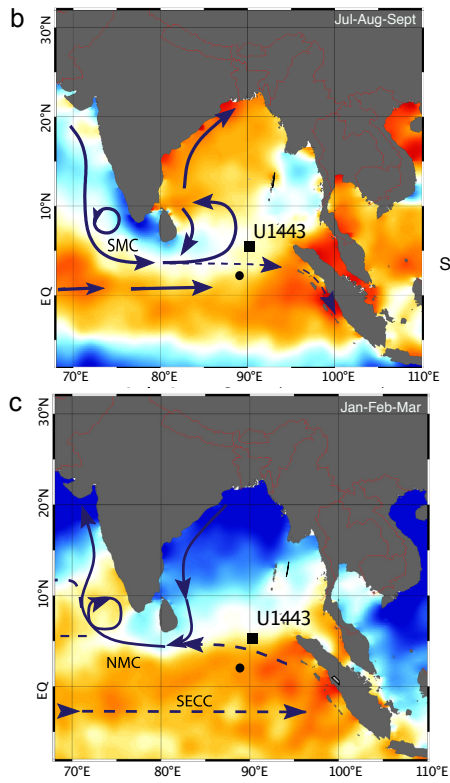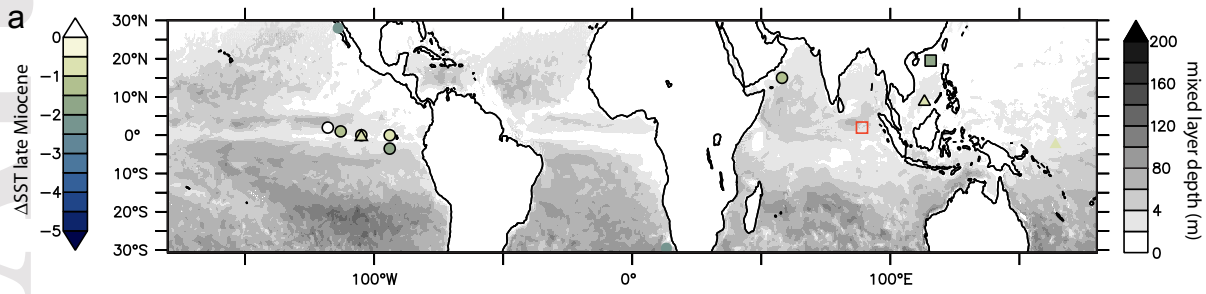
Zhu, J., Poulsen, C. J., & Tierney, J. E. (2019). Simulation of Eocene extreme warmth and high climate sensitivity through cloud feedbacks. *Science advances*, *5*(9), eaax1874. DOI: 10.1126/sciadv.aax1874

Zhuang, G., Pagani, M., & Zhang, Y. G. (2017). Monsoonal upwelling in the western Arabian Sea since the middle Miocene. *Geology*, *45*(7), 655-658. https://doi.org/10.1130/G39013.1

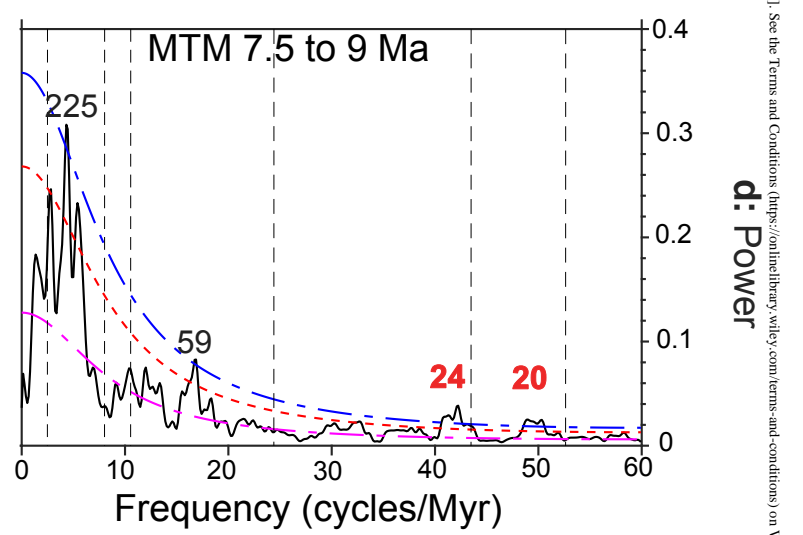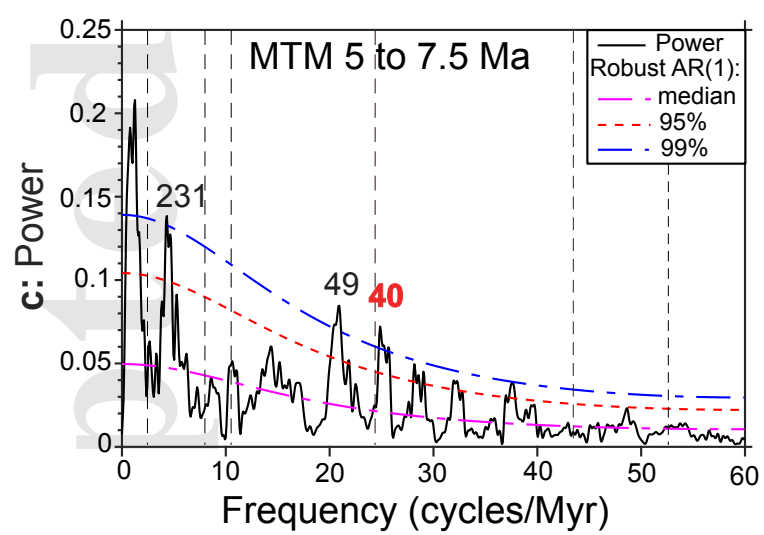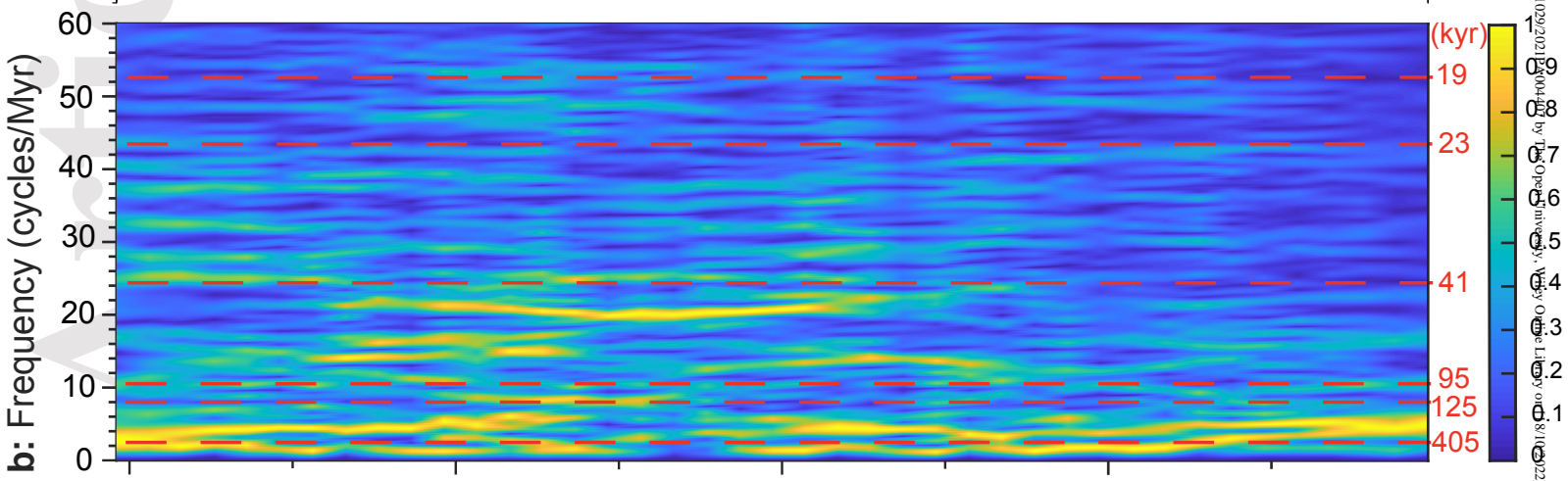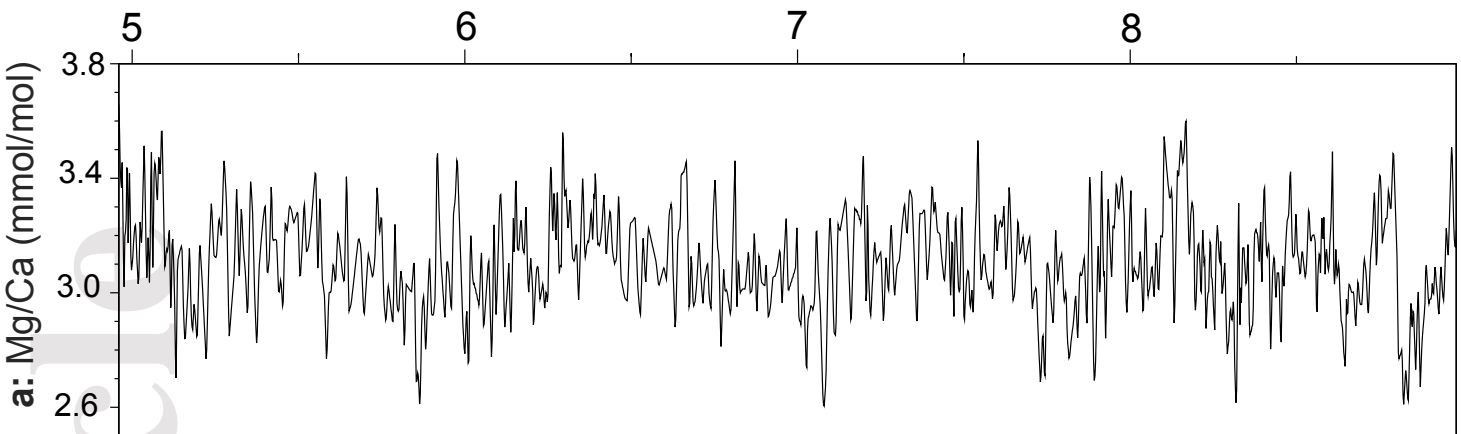Zweng, M. M., J. R. Reagan, D. Seidov, T. P. Boyer, R. A. Locarnini, H. E. Garcia, A. V. Mishonov, O. K. Baranova, K. Weathers, C. R. Paver, and I. Smolyar, 2018. *World Ocean Atlas 2018, Volume 2: Salinity*. A. Mishonov Technical Ed.; NOAA Atlas NESDIS 82, 50pp. http://doi.org/10.7289/V5251G4D
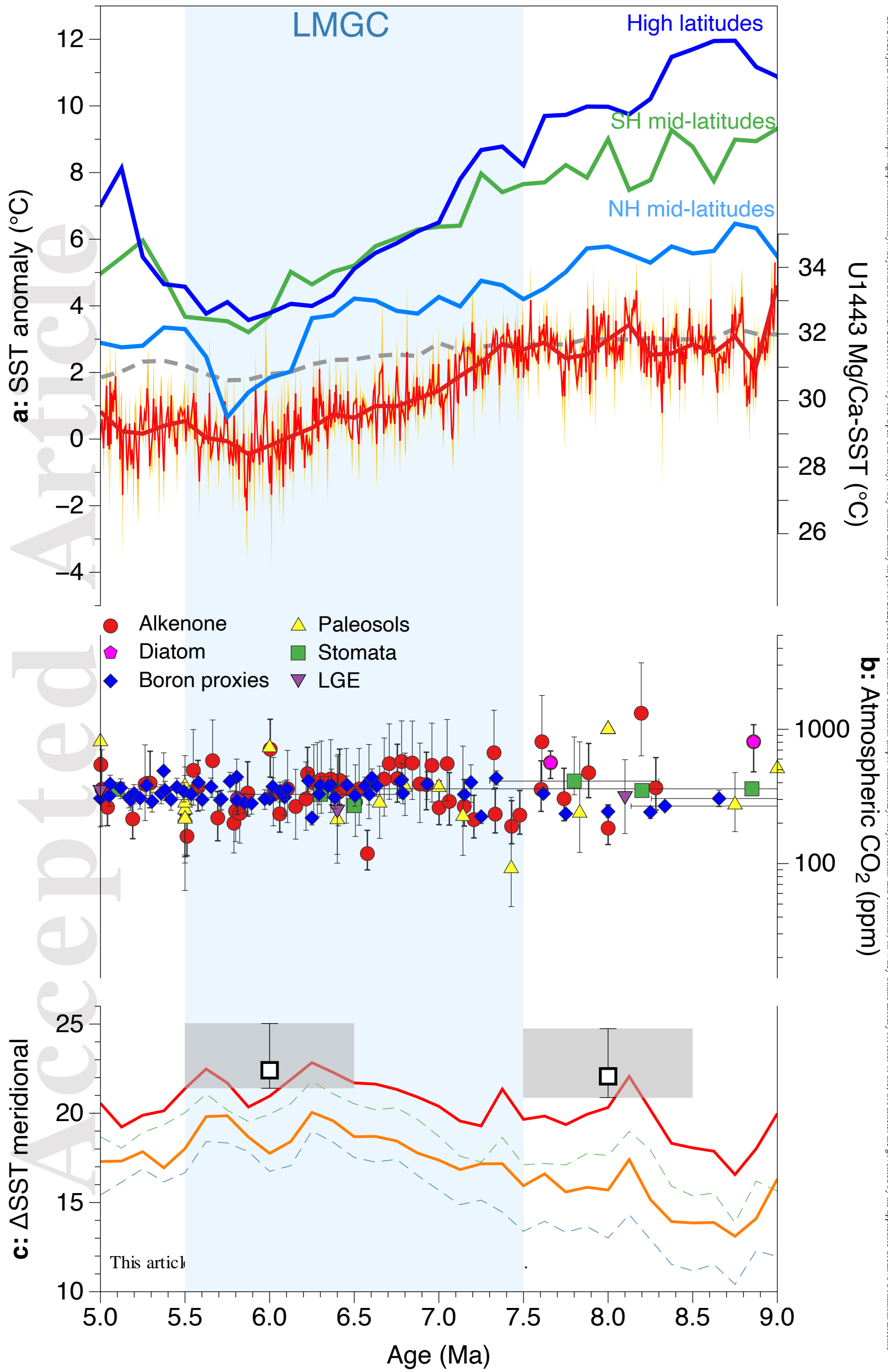
**a:** SST anomaly (°C)

LMGC

High latitudes

SH mid-latitudes

NH mid-latitudes

U1443 Mg/Ca-SST (°C)

**b:** Atmospheric CO$_2$ (ppm)

- 🔴 Alkenone
- 🔷 Diatom
- 🔷 Boron proxies
- 🔺 Paleosols
- 🟩 Stomata
- 🔻 LGE

**c:** ΔSST meridional

This article
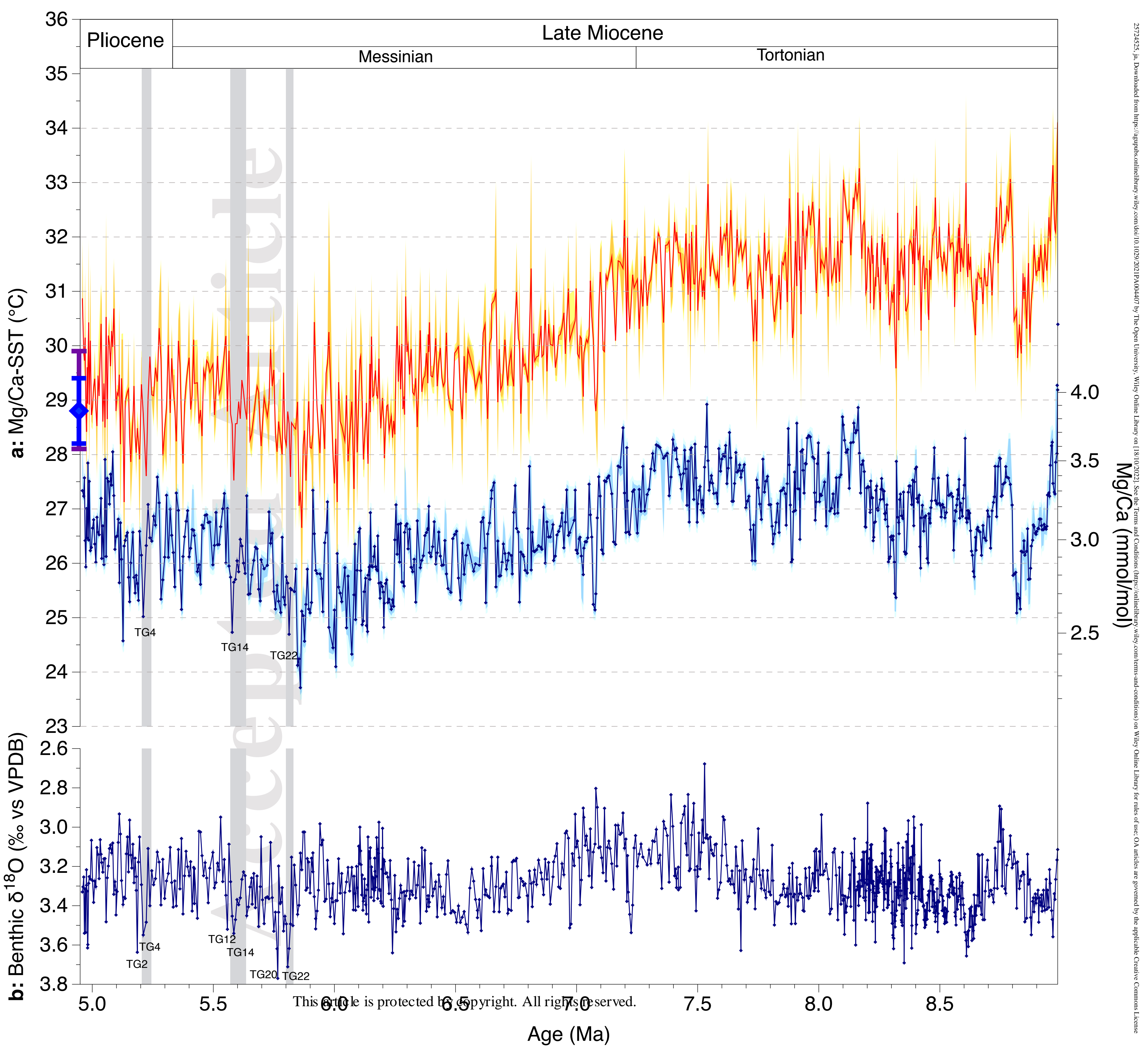
Age (Ma)
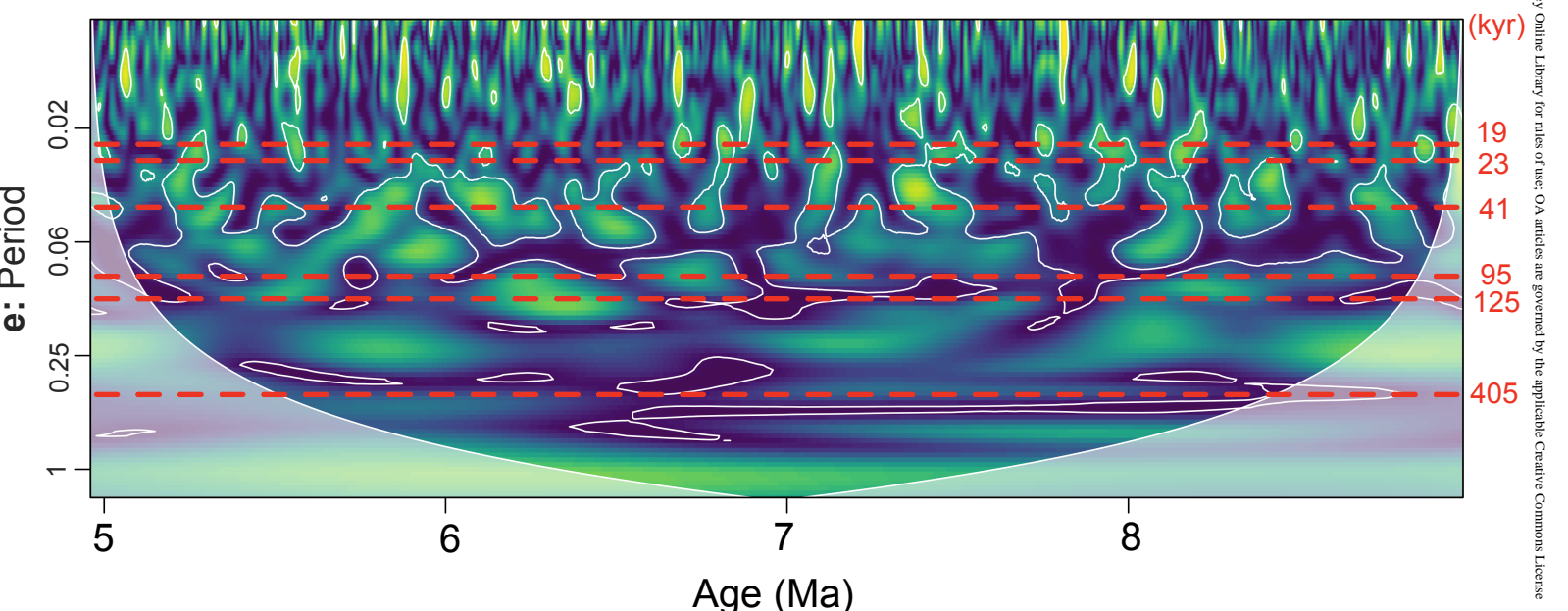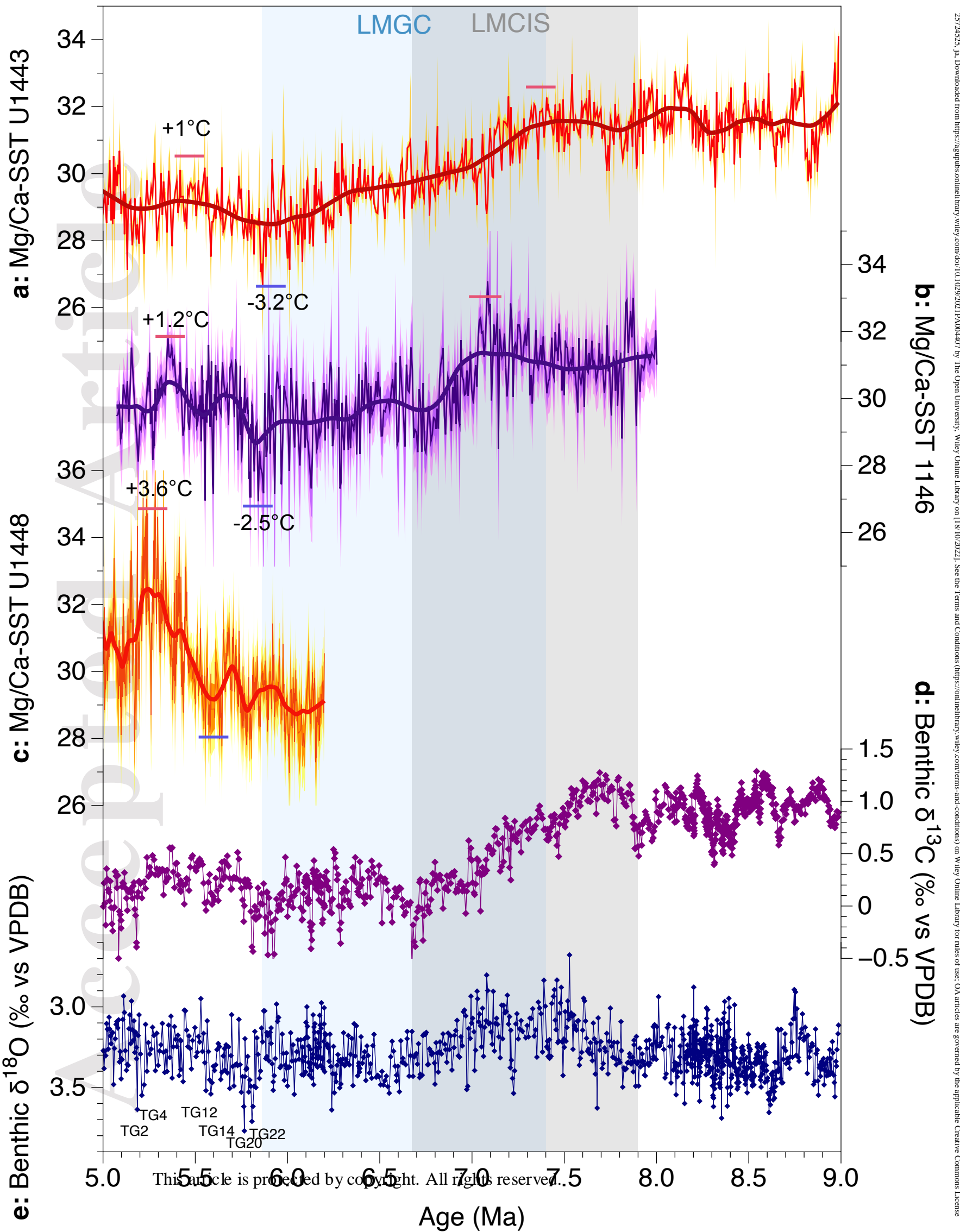
## 6 Ma ±0.5 ($CO_2$ 300 ppm, LM paleoceanography)

Legend:
- Modelled SSTs gradient LM-300
- Model error max/min SSTs LM-300
- ☆ Mg/Ca-SST
- ○ $U_{37}^{k}$-SST
- ◇ TEX$_{86}$-SST
- ■ Pacific
- ■ Atlantic
- ■ Indian

Y-axis: Mean SST (°C)
X-axis: Latitude
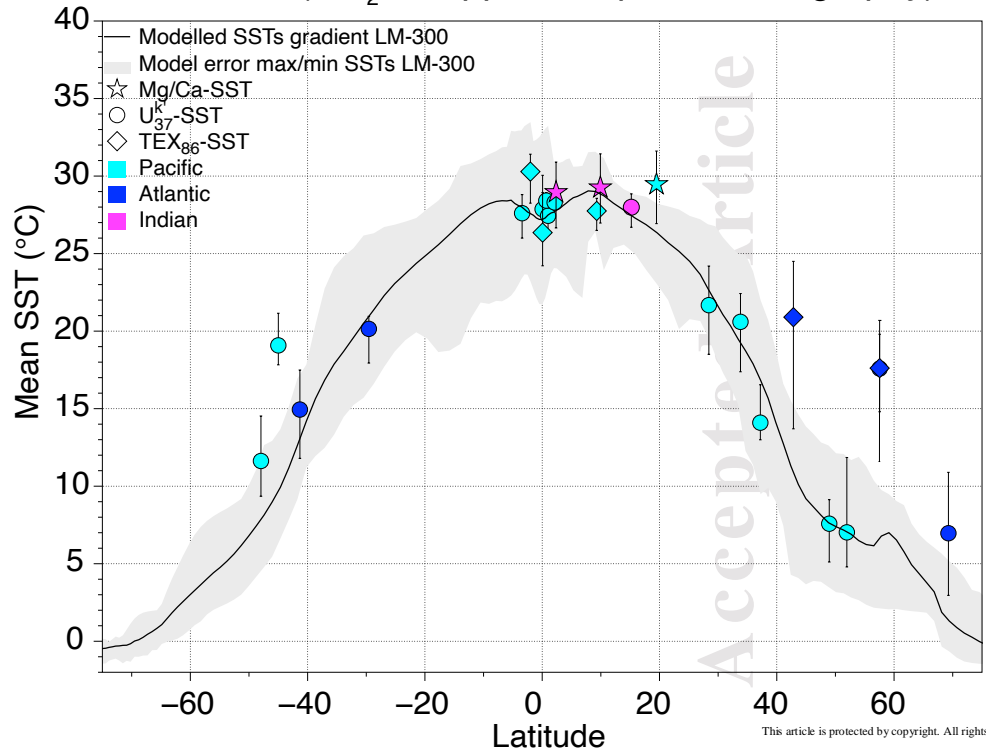
## 8 Ma ±0.5 ($CO_2$ 560 and 420 ppm, LM paleoceanography)

Legend:
- Modelled SSTs gradient LM-560
- Modelled SSTs gradient LM-420
- Model error max/min SSTs LM-560
- ☆ Mg/Ca-SST
- ○ $U_{37}^{k}$-SST
- ◇ TEX$_{86}$-SST
- ■ Pacific
- ■ Atlantic
- ■ Indian

Y-axis: Mean SST (°C)
X-axis: Latitude